THESIS FOR THE DEGREE OF DOCTOR OF PHILOSOPHY

in

Thermo and Fluid Dynamics

Experimental Studies on Using Butanol and Octanol Isomers as Drop-in Fuels for Diesel Engines

TANKAI ZHANG

Department of Mechanics and Maritime Sciences
CHALMERS UNIVERSITY OF TECHNOLOGY
Gothenburg, Sweden, 2019

Experimental Studies on Using Butanol and Octanol Isomers as Drop-in Fuels for Diesel Engines
TANKAI ZHANG
ISBN 978-91-7597-880-2

Doktorsavhandlingar vid Chalmers tekniska högskola
Ny serie nr 4561
ISSN 0346-718X

Department of Mechanics and Maritime Sciences
Chalmers University of Technology
SE-412 96 Gothenburg
Sweden
Telephone +46 (0)31 772 1000

Chalmers Reproservice
Gothenburg, Sweden 2019

Experimental Studies on Using Butanol and Octanol Isomers as Drop-in Fuels for Diesel Engines

TANKAI ZHANG

Department of Mechanics and Maritime Science
Chalmers University of Technology

Abstract

The increasing importance of transportation in modern societies has caused fossil fuel consumption to increase greatly in recent decades. However, burning fossil fuels in internal combustion engines can lead to high emissions of greenhouse gases, which cause climate change. Because of this, there is great interest in using alcohols and other renewable fuels in Diesel engines to reduce vehicles' lifecycle greenhouse gas emissions. It is therefore important to investigate the possibility of using alcohol/Diesel blends, or even fossil-free blends, in both existing Diesel engines and new engines employing advanced combustion concepts.

This thesis explores the use of four alcohols (*n*-butanol, isobutanol, 2-ethylhexanol, and *n*-octanol) and two bio-Diesels (hydrotreated vegetable oil, or HVO, and rapeseed methyl ester) as drop-in fuels in Diesel engines. Their effects on the performance and emissions of compression ignition engines were assessed by performing experiments using light- and heavy-duty single cylinder engines under steady-state conditions.

To test the compatibility of alcohol-containing blends with existing engines, HVO and the commercial cetane number (CN) improver DTBP were used to compensate for the alcohols' low CN values and prepare oxygenated blends with CN values similar to fossil Diesel. Blends with and without fossil Diesel were tested. Two single-cylinder engines were operated at four standard load points using production calibrated engine settings. Experiments were also performed using an advanced combustion strategy (partially premixed combustion) in which the alcohols were blended with fossil Diesel fuel directly to produce mixtures with low cetane numbers (26 or 36). The blends' effects on spray penetration, flame development, and soot characteristics were investigated in the constant volume combustion chamber.

The results show that from a combustion point of view, the tested alcohol blends with Diesel-like CN values can be used in unmodified existing Diesel engines. Compared to conventional Diesel fuel, the oxygenated blends yielded slightly higher indicated thermal efficiencies, significantly lower soot emissions, and similar heat release profiles. Moreover, partially premixed combustion was shown to further increase thermal efficiency while reducing soot and NO_x emissions.

List of publications

This thesis is based on the work contained in the following papers:

I. T. Zhang, K. Munch, and I. Denbratt, "An Experimental Study on the Use of Butanol or Octanol Blends in a Heavy Duty Diesel Engine," *SAE Int. J. Fuels Lubr.*, 8(3): 2015-24-2491, 2015.

II. T. Zhang, L. J. Nilsson, C. Björkholtz, K. Munch, and I. Denbratt, "Effect of Using Butanol and Octanol Isomers on Engine Performance of Steady State and Cold Start Ability in Different Types of Diesel Engines," *Fuel*, 184:708–717, 2016.

III. T. Zhang, K. Munch, and I. Denbratt, "Combustion Characteristics for Partially Premixed and Conventional Combustion of Butanol and Octanol Isomers in a Light Duty Diesel Engine," *SAE Technical Paper*, 2017-01-2322, 2017.

IV. T. Zhang, M. Andersson, K. Munch, and I. Denbratt, "Optical Diagnostics on Spray Characteristics and Soot Volume Fraction of n-butanol, Diesel and Hydrotreated Vegetable Oil Blends in a Constant Volume Combustion Chamber," *SAE Technical Paper*, 2019-01-0019, 2019.

V. T. Zhang, J. Eismark, K. Munch, and I. Denbratt, "Effects of a Wave-Shaped Piston Bowl Geometry on the Performance of Heavy Duty Diesel Engines Fueled with Alcohols and Biodiesel Blends," manuscript submitted to journal *Fuel* in February 2019.

Other related work:

VI. K. Munch and T. Zhang, "A Comparison of Drop-In Diesel Fuel Blends Containing Heavy Alcohols Considering Both Engine Properties and Global Warming Potentials," *SAE Technical Paper*, 2016-01-2254, 2016.

Contents

Nomenclature

A/F ratio	Air/fuel ratio
ATDC	After top dead center
BTDC	Before top dead center
BTL	Biomass to liquid
CAD	Crank angle degrees
CFR	Co-operative fuel research
CI	Compression ignition
CLD	Chemiluminescence detector
CN	Cetane number
CO	Carbon monoxide
CO_2	Carbon dioxide
COV	Coefficient of variation
DCN	Derived cetane number
DI	Direct injection
DTBP	Di-tertiary-butyl peroxide
EGR	Exhaust gas recirculation
EOI	End of injection
FAME	Fatty acid methyl ester
FID	Flame ionization detector
FIT	Fuel ignition testing
FSN	Filter smoke number
GHG	Greenhouse gas
H_2	Hydrogen
HC	Hydrocarbon
HCCI	Homogeneous charge compression ignition
HD	Heavy duty
HVO	Hydrotreated vegetable oil
ID	Ignition delay
IMEP	Indicated mean effective pressure
IQT	Ignition quality tester
IRD	Infrared detector
ITE	Indicated thermal efficiency
IVC	Inlet valve closing
LD	Light duty
LTC	Low temperature combustion
LOL	Lift-off length
LVH	Low heating value
NIR	Near infra-red
NGL	Natural gas liquid
NO	Nitric oxide
NO_x	Nitrogen oxides
PPC	Partially premixed combustion
ppm	Parts per million
PM	Particulate matter
PN	Particulate number
RME	Rapeseed methyl ester
Rpm	Revolutions per minute
SOC	Start of combustion
SOI	Start of injection
TDC	Top dead center
Vol.	Volume
Wt.	Weight
WTW	Well to wheels

1 Introduction

1.1 Motivation

In recent decades, modern societies rely heavily on internal combustion engines for transportation because of the wide range of available engine sizes and the lack of similarly capable alternatives. The growing demand for transportation has expanded the global market for internal combustion engines. In 2016, the global population of engine-powered vehicles reached around 1.32 billion, [1,2] of which 295.7 million were located in the European Union. Around 99.8 % of these vehicles have an internal combustion engine. [3]

The ubiquitous use of internal combustion engines has contributed significantly to the production of greenhouse gas (GHG) emissions generated by burning fossil fuels, which cause global climate change. In the EU-28, the transportation sector accounted for 24 % of all GHG emissions in 2016. [4] In the US, transport accounted for 28 % of all GHG emissions (1551 million tonnes of CO_2 equivalents) and was the largest single source of greenhouse gas emissions in 2016. [5] Despite of the high share, GHG emissions due to transport appear to be increasing in the EU and the US as a proportion of overall emissions and there is no reducing trend in absolute terms.

The European Union has made a commitment to reduce the overall GHG emissions of its 28 Member States by 20 % relative to 1990 levels by 2020 [6].The intent is to then reduce GHG emissions by at least 40 % relative to 1990 levels by 2030 [7] and 80 – 95 % by 2050 [8].

Another drawback of high fossil fuels consumption relates to the contradiction between great demand and uneven distribution of oil escalates the international tensions and conflicts. As societies have developed, peoples' daily lives have become increasingly dependent on the use of fossil fuels. ***Figure 1-1*** shows the EU's import dependency of energy by fuel between 1990 and 2016. The import dependency is defined as the ratio of dependency on importation in relation to domestic consumption. The union's overall import dependency on all fuels increased by 24.3 % during between 1990 and 2008 (from 45.2 % to 56.2 %). Furthermore, the union's dependence on imports of crude oil and natural gas liquid (NGL) increased from 78.6 % in 1990 to 87.4 % in 2016. Oil reserves tend to occur in relatively concentrated pockets across the world. For instance, the countries with the eight largest oil reserves collectively owned 79.4 % of the world's proven oil reserves at the end of 2014. [9] The high import dependency along with the low reservation could cause national security issues. However, renewable fuels are less import dependent because they can be produced from diverse feedstocks.

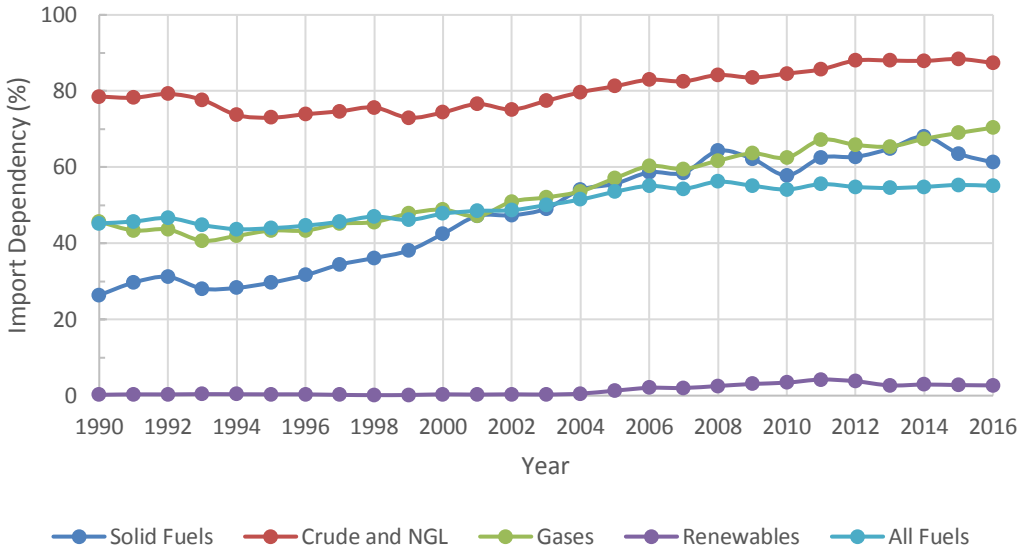

Figure 1-1 EU-28 energy import dependency (in %) by fuel (1990 - 2016) [10]

To enhance energy security and reduce GHG emissions, the European Union has pledged to increase the proportion of energy generated from renewable resources within the transportation sector to 10 % by 2020, with the overall share of energy generated from renewable sources rising to 20 %. [7] By 2030, the intent is for 14 % within the transportation sector and 32 % of all energy demand to be met by renewable sources. [11] However, this is an overall target; each European country is free to implement its own policies to work towards these goals. Sweden aims to reduce 70 % climate impact from transport sector by 2030 relative to 2010, and to achieve a net zero GHG emissions by 2045. [12]

Figure 1-2 shows the roadmap for the EU's 2050 energy strategy. The coloured bars in this figure indicate the expected ranges of the shares of primary energy consumption in 2030 and 2050 under various decarbonisation scenarios. The projected share of renewable energy sources (RES) in 2050 exceeds that of all other primary sources.

In the transportation sector, efforts to reduce GHG emissions are complicated by the existence of vast numbers of internal combustion engine vehicles. Therefore, efforts have been made to replace fossil fuels with renewable alternatives. In China, E10 fuel (10 % ethanol in gasoline) is currently sold in 11 provinces and will be sold nationwide by 2020 and cellulosic ethanol production is projected to overtake crop ethanol production by 2025, further reducing the environmental impact of ethanol blends. [13] In the US, the American Recovery and Reinvestment Act of 2009 requires the share of ethanol in gasoline to rise from 7 % to 10 %, and it is expected to remain at the latter level until 2030. [14] In Canada, a federal mandate has

required 5 % of the national gasoline pool to be renewable (ethanol) since 2010. [15] In addition, some provinces have mandated equivalent or higher renewable fuel contents: 5 % in Ontario, 7.5 % in Saskatchewan, and 8.5 % in Manitoba.

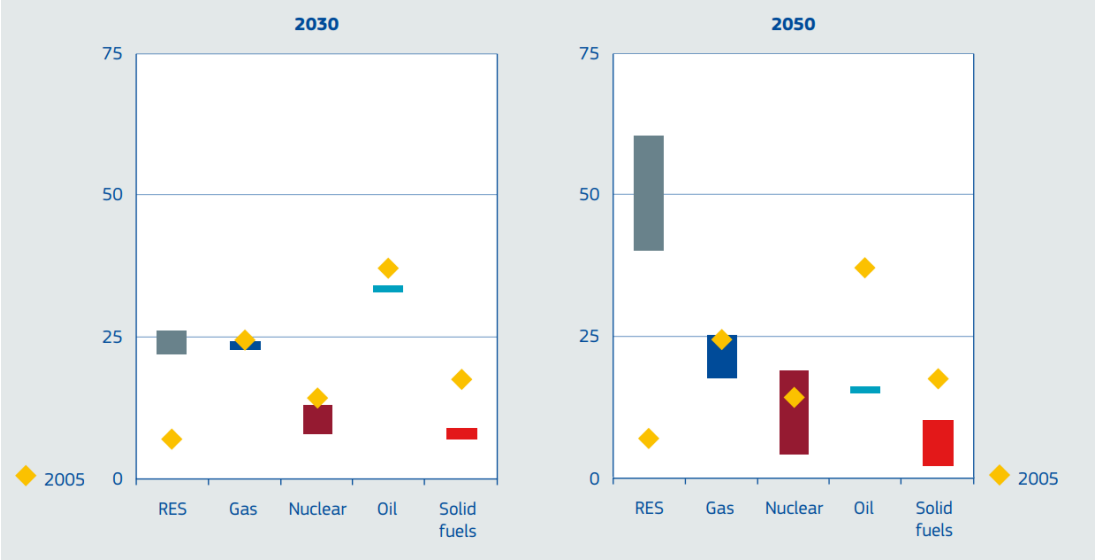

Figure 1-2 Shares of overall primary energy use for different fuels in 2030 and 2050. Yellow diamonds indicate the shares for each fuel in 2005. [16]

1.2 Objective

GHG emissions from engines can be reduced by replacing fossil fuels with biofuels and by increasing the engines' thermal efficiency. The use of biofuels is an attractive option that could reduce vehicles' 'well to wheel' GHG emissions to comply with increasingly stringent regulations. Thermal efficiency could be increased by using new technologies such as advanced combustion strategies or optimized combustion system design. Combined the two pathway above, can alcohols be used in non-modified Diesel engines or advanced combustion system as drop-in fuels?

The main objective of the work presented was to investigate the possibility of using alcohol/Diesel blends coupled with ignition improvers in existing engines and the potential of applying low cetane numbers (CN) alcohol/Diesel blends in partially premixed combustion (PPC) aim for a high thermal efficiency of Diesel engine.

It is essential to evaluate the performance and emissions of unmodified existing vehicles with partially replacing Diesel fuel by renewable alcohols. To evaluate their potential, *n*-butanol, isobutanol, *n*-octanol, and 2-ethylhexanol were selected to blend with Diesel fuel for

conventional compression ignition (CI) combustion. The CNs of the different alcohol/Diesel blends were adjusted to match that of Diesel by adding two different CN improvers: hydrotreated vegetable oil (HVO) and di-tertiary-butyl peroxide (DTBP). Because of the tested blends had identical CNs, they also had similar ignition delays (IDs). Conventional CI combustion experiments were performed in a single cylinder heavy duty (HD) engine and a single cylinder light duty (LD) engine. Cold start tests were performed in a multi-cylinder LD engine.

In addition to the conventional CI combustion experiments, partially premixed combustion was studied in LD and HD single cylinder engines fuelled with Diesel-alcohol (*n*-butanol, isobutanol, *n*-octanol, and 2-ethylhexanol) blends without any CN improvers. To optimize combustion, the exhaust gas recirculation (EGR) level, lambda, and injection strategy were tuned for each blend separately. The measured emissions and thermal efficiencies for each blend during PPC were compared to those for conventional CI combustion using production engine settings.

The effects of using *n*-butanol, *n*-octanol, fossil Diesel, hydrotreated vegetable oil (HVO), and blends of these fuels on spray penetration, flame development, and soot characteristics were investigated in a high-pressure high-temperature constant volume combustion chamber designed to mimic a heavy duty Diesel engine. Backlight illumination was used to capture liquid and vapor phase spray images with a high-speed camera. The flame lift-off length (LOL) and ignition delay were determined by analyzing OH* chemiluminescence images. Laser extinction diagnostics were used to measure the spatially and temporally resolved soot volume fraction. The spray experiments were performed by injecting fuels under non-combusting (623 K) and combusting (823 K) conditions at a fixed ambient air density of 26 kg/m^3.

2 Background

2.1 Alternative fuels

2.1.1 Alcohols

Alcohols can be produced from sugar cane, switchgrass, corns and other starch-rich materials by fermentation. They can also be generated sustainably from CO_2 and H_2 as so-called electrofuels [17] or from non-food lignocellulosic biomass. Lignocellulosics has three major components: cellulose, hemi-cellulose, and lignin. Alcohol production from lignocellulosics typically involves two main steps: hydrolysis of cellulose and hemicellulose to monomeric sugars, which are then fermented to produce bio-alcohol. [18,19]

Lifecycle assessments indicate that converting waste bioresources into fuel for internal combustion engines could be an excellent way of achieving extremely low life-cycle GHG emissions. For instance, replacing fossil fuels with ethanol produced from wheat can reduce well-to-wheels (WTW) typical GHG emissions by 32 - 53 % [20], while produced from waste wood the figure could be 80 - 87 %. [21] Methanol and butanol produced from inedible feedstocks can also be used as alternative fuels, and similarly have the potential to reduce WTW typical GHG emissions substantially (by 70 – 90 %). [21, 22]

The physical properties of alcohols make them potentially suitable fuels for Diesel engines. ***Table 2-1*** shows some key physicochemical properties of alcohols and fossil Diesel.

Table 2-1 Properties of alcohols and Diesel [23,24,25,26]

	Methanol	Ethanol	Isobutanol	*n*-Butanol	2-Ethylhexanol	*n*-Octanol	Diesel
Oxygen content (wt.%)	49.93	34.73	21.62	21.62	12.31	12.3	0
Density (g/ml)	0.787	0.785	0.802	0.810	0.836	0.830	0.837
Lower heating values (MJ/kg)	20.1	26.9	33.2	33.2	34.7	38.4	42.8
Cetane number	3.8	5-8	< 15	< 20	23.2	37.5	52
Flash point (°C)	12	13	28	35	77	81	82
Vaporization latent heat (kJ/kg)	1109	904	566	582	358	562	270
Boiling point (°C)	65	79	108	118	184	195	193-357
Viscosity @ 40 °C (mm^2/s)	0.58	1.13	2.62	2.63	5.2	5.5	3.04
Lubricity (μm)	1100	1057	-	590	-	236	315
Solubility in water	Miscible	Miscible	Immiscible	Immiscible	Immiscible	Immiscible	Immiscible

Alcohols are compounds having a chain of carbon atoms bound to a hydroxyl group (-OH). Their physical and chemical properties depend heavily on the number of carbon atoms in the chain and their molecular structure. As the number of carbon atoms in the chain increases, the alcohol's oxygen content decreases (on a wt. % basis) while that of carbon increases. Increasing the carbon content generally increases the lower heating value (LHV) and thus reduces specific fuel consumption. The alcohols used in this study all have lower LHVs than fossil Diesel, so the output of an engine burning these alcohols would be lower than that of burning Diesel for a given quantity of injected fuel. However, engines burning long chain alcohol/Diesel blends can achieve similar maximum outputs to those achieved with Diesel fuel [27]. Straight carbon chain alcohols have slightly higher LHVs than their branched isomers.

Increasing the number of carbon atoms in alcohols reduces their molecular latent heat of vaporization but increases their boiling point and density, making their properties more similar to those of Diesel. The latent heat of vaporization influences the temperature in the cylinder after the injection, especially in the region surrounding the spray. [28] The lower density of alcohols leads to a lower energy density, which complicates their use in existing Diesel engines when the fuel tank volume is fixed.

Compared to ethanol and methanol, alcohols with longer carbon chains have higher CNs and flash points that are closer to the limits specified in the EN590 Diesel standard. This should facilitate their integration into existing fuel supply chains. The CN has a strong effect on the ID and significantly affects combustion behaviour; consequently, long-chain alcohols behave more like Diesel during combustion than do ethanol and methanol. The lower limit on the flash point specified in the EN 590 Diesel standard is 55 °C; whereas the flash points of ethanol and methanol are well below this limit, the flash points of *n*-Octanol (81 °C) and 2-ethylhexanol (77 °C) are comfortably above it, making them safer to distribute and store.

The hydrophilicity of ethanol makes it insoluble in Diesel, so emulsifiers must be added to ethanol/Diesel blends, which complicates the preparation of the fuels. The physical properties of butanol isomers and octanol isomers make them more suitable than methanol or ethanol as alternative fuels to blend with fossil Diesel.

Fuels' lubricative properties are typically tested using a high frequency reciprocating rig to measure the wear scar diameter, which should not exceed 460 µm according to the EN590 standard. Poor lubricity can cause wear problems in the fuel pumps and injector. Alcohols with higher carbon numbers have greater lubricity; *n*-octanol complies with the requirements of EN590 in this respect.

2.1.2 Other alternative Diesel fuels

Commercially available fatty acid methyl ester (FAME) blends in Diesel are mainly made from animal fats and some vegetable oils by an esterification process. [29] Diesel fuel sold in Sweden may contain up to 7 % FAME. A commonly used FAME is rapeseed methyl ester (RME), which has very favourable lubricity [30], a high oxygen content, and a Diesel-like CN, but poor cold properties.

Hydrotreated vegetable oil (HVO) is a high CN biofuel with properties similar to Diesel fuel. It is a mixture of straight- and branched-chain paraffins that are refined from the wider feedstock than FAME. Moreover, the advances in HVO refining techniques have enabled the production of fuels containing no aromatics or sulphur [31,32].

2.2 Methods for introducing alcohol-based fuels into Diesel engines

Depending on their fuel properties and the chosen combustion control strategy, alcohols can be introduced into engines separately from Diesel or as drop-in fuel in Diesel. The use of separate injection systems for alcohols and Diesel allows combustion behaviour to be controlled by adjusting the relative proportions of each fuel, in the so-called dual fuel operating mode. [33] It can be difficult to control the auto-ignition timing when using premixed combustion strategies such as homogeneous charge compression ignition (HCCI), which limits the range of operating conditions compatible with such strategies. The use of alcohols together with Diesel in dual fuel mode can overcome the auto-ignition timing problems and extend the operating range, improving fuel economy and greatly reducing NO_x and soot emissions [34]. However, the drawbacks are its relatively high CO and HC emissions [35] and the cost of a separate injection system.

An alternative to dual fuel operation is the so-called drop-in fuel, in which a blend of alcohol and Diesel fuel is injected directly into the cylinder. This may not requires modification of the engine hardware. However, emulsifiers must be added to blends containing short carbon chain alcohols (e.g. methanol or ethanol), which are otherwise insoluble in Diesel fuel.

In experiments comparing dual fuel and blend mode operation using *n*-butanol and Diesel fuel, port injection of *n*-butanol in dual fuel mode resulted in fuel pooling in the intake and incomplete combustion, causing higher CO emissions than blend mode operation.[36]. In addition, dual fuel operation generated higher HC emissions than blend operation because of more extensive quenching at low combustion temperatures. Increased CO and HC emissions are associated with reduced combustion efficiency, which may lead to a lower indicated thermal efficiency (ITE). ***Figure 2-1*** shows soot-NO_x trade-off curves for a Diesel engine operating at

1800 rpm and 95 Nm in three different operating modes - butanol/Diesel blend direct injection (BF), butanol/Diesel duel fuel injection (PI), and Diesel direct injection (DF). [37] The dual fuel and blended fuel methods both yielded lower soot-NO_x trade-off curves than conventional Diesel direct injection, and the blended fuel showed better performance than the duel fuel mode. The smoke-reducing effect of butanol was thus attributed to both its oxygen content and its tendency to increase the ID. Butanol/Diesel blends also exhibit more favourable spray characteristics than pure Diesel because of butanol's low surface tension and boiling point. However, it has been suggested that the low CN of such blends may cause problems during cold starts.

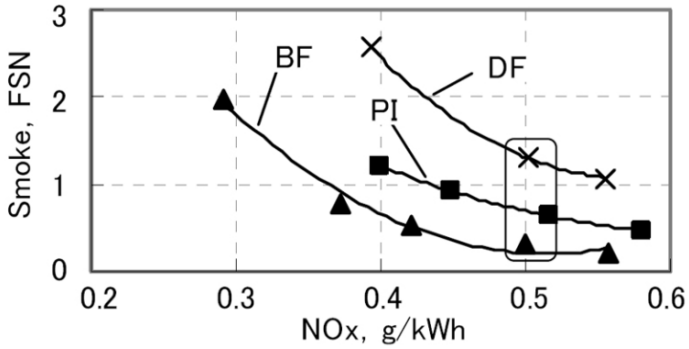

Figure 2-1 The trade-off between smoke and NO_x emissions (1800 rpm, 95 Nm) [37]

Because it requires engine modifications, dual fuel mode is less easily implemented in existing Diesel engines than operation using alcohol/Diesel blends. Therefore, the alcohol/Diesel blend method has distinct advantages for use in existing engines.

2.3 Application of alcohol/Diesel blends

Four types of compression ignition strategies can be delineated based on the injection timings that they use: conventional CI combustion, partially premixed combustion (PPC), premixed charge compression ignition (PPCI), and HCCI. Because of their good volatility, and other favourable properties, alcohol-based fuels are compatible with all these strategies. This thesis focus on the use of alcohol-based fuels in conventional CI combustion and PPC.

2.3.1 Effect of alcohol/Diesel blends for conventional CI combustion

Alcohols have lower LHVs than Diesel fuel. Consequently, the use of Diesel blends containing 30 % butanol or 25 % pentanol in Diesel engines reduced their maximum output by 4 % and 3%, respectively, compared to operation using neat Diesel. [38] These reductions in output were smaller, in relative terms, than the differences in LHV between the blends and neat Diesel. This

is presumably because the oxygen content of the blends promotes complete combustion, increasing the engine's thermal efficiency; this partially compensates for the blends' lower LHVs. However, Can et al. [39] reported that adding 10 or 15 % ethanol to Diesel fuel with an emulsifier reduced engine power by approximately 12.5 % or 20 %, respectively. These declines were greater than the reductions due to ethanol's low LHV and density, which was attributed to an inefficient conversion of heat into work due to a longer ID, leading to late heat release during the expansion stroke and loss of effective expansion.

The alcohol/Diesel blends yielded lower soot and CO emissions than Diesel fuel. [40,41] This may be primarily due to the presence of fuel-bound oxygen in locally rich 'zones' in the combustion chamber. The longer ID resulting from the use of alcohol/Diesel blends may increase the proportion of the fuel that is burned during the premixed combustion phase, explaining much of the observed low soot emissions[42]. The fuel-bound oxygen in alcohols may also enhance the oxidation of soot precursors in fuel-rich core regions of the fuel spray. Fuel properties such as the viscosity and boiling points, surface tension and density affect spray properties, and the fuel's C/H ratio may influence particulate matter formation. [43] Butanol/Diesel blends yield longer flame lift-off lengths than Diesel under identical conditions, allowing more space and time for air entrainment upstream of the spray. [44] This leads to a better air-fuel mixing, reducing the equivalence ratio in the combustion region and thereby suppressing soot formation and promoting soot oxidation. [45]

The use of alcohol/Diesel blends also affects NO_x emissions. Butanol/Diesel blends tend to yield 'leaner' combustion with lower combustion temperatures than pure Diesel. Importantly, butanol's low LHV and high heat of evaporation (compared to Diesel fuel) tend to outweigh the effects of increased local oxygen concentration and enhanced premixed combustion, which would otherwise favour NO_x formation. [46] Consequently, NO_x emissions from engines using Diesel/butanol blends are usually slightly lower than those achieved with pure Diesel. However, Valentino et al. [47] reported that *n*-butanol/Diesel blends generated higher NO_x emissions than neat Diesel when burned in a four-cylinder LD Diesel engine. This outcome may be related to the ID and the alcohol's cooling effect. If the SOI timing used with alcohol/Diesel blends is identical to that used with neat Diesel, the CA50 will occur at a later crank angle when using the blends, reducing the combustion temperature and NO_x emissions. However, if the difference in CA50 is small enough, the higher combustion temperatures resulting from the blends' tendency to enhance premixed combustion will outweigh the alcohol's cooling effect, increasing NO_x emissions.

Injection pressure has more impact on the NO_x emissions than soot and HC emissions, when using *n*-butanol/Diesel blends. [48] NO_x emissions increase with injection pressure, especially

for blends with high *n*-butanol/Diesel ratios. The injection strategy influences the effect of adding alcohol. Both multi-injection strategies and the use of a butanol/Diesel blend were shown to reduce soot emissions. However, when both strategies were implemented together, their combined effect was weaker than that of either strategy alone. [49]

Figure 2-2 [50] shows soot emissions as functions of the EGR rate for neat Diesel and blends of Diesel with *n*-butanol. Soot formation peaked at EGR rates between 45 and 65 %. The butanol blends reduced soot formation, especially in this heavily sooting region.

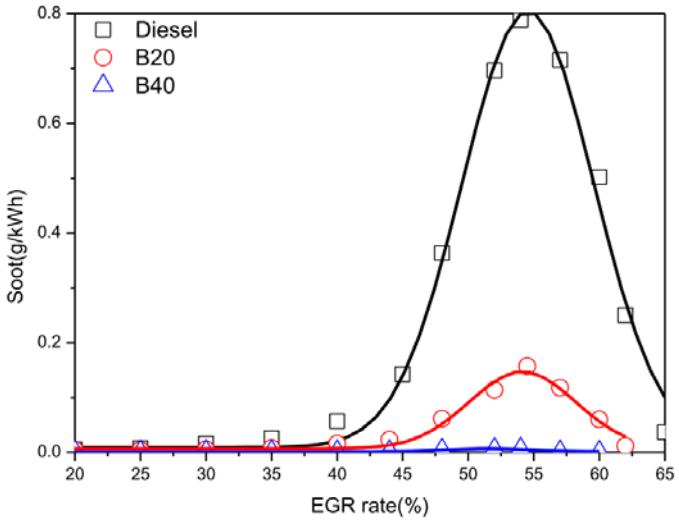

Figure 2-2 Soot emissions achieved with neat Diesel and blends containing 20 or 40 wt .% n-butanol (B20 and B40, respectively) as functions of the EGR rate.

Exhaust emissions after engine cold/warm starts were investigated in a turbocharged 4-cylinder direct injection (DI) Diesel engine fuelled with an ethanol (10 %)/Diesel blend or a butanol (16 %)/Diesel blend [51]. Both blends increased specific NO_x, HC, CO, and smoke emissions under cold start conditions. This was attributed to the alcohols' high latent heat of vaporization, which can lead to a low cylinder temperature, incomplete combustion, and poor oxidation. Armas et al.[52] studied emissions under the New European Driving Cycle using the same blends, revealing that over the entire driving cycle, the blends generated lower soot and CO emissions than Diesel fuel but higher NO_x and HC emissions.

2.3.2 Effect of alcohol/Diesel blends for partially premixed combustion

PPC usually requires a slightly earlier fuel injection than conventional combustion to give enough time for mixing to ensure that the start of combustion (SOC) occurs after the end of injection (EOI). Partially premixed combustion has shown the potential of increasing thermal

efficiency while reducing engine out NO_x and soot emissions relative to conventional combustion. [53] A common way of achieving PPC is to use a low compression ratio and high levels of cooled EGR, which increases the ignition delay time and the heat capacity of the gas in the cylinder, resulting in a less fuel rich region and a lower combustion temperature and thereby avoiding the high soot and NO_x production zone [54]. However, PPC could also be achieved by adjusting the fuel's CN to increase the ID and enable more homogeneous premixed fuel air mixture [55,56].

PPC combustion using blends with high *n*-butanol/Diesel ratios (50 to 100 %) yielded gross indicated efficiencies above 50 % over a wide load range, with the 60 % blend performing particularly well. [57] However, incomplete combustion caused higher HC and CO emissions than were observed during conventional combustion. [58] Emissions of NO_x, CO, and HC during PPC do not depend directly on the fuel's CN; instead, they depend on the ID, which is affected by the CN but also by factors such as the EGR rate. [59]

2.4 CN of the fuel

The cetane number is a dimensionless index that is related to the ID, i.e. the period between the start of injection (SOI) and start of combustion (SOC). It can be used to quantify the quality of ignition and the heat release phase.

2.4.1 Effect of CN on combustion

The CN has significant effects on emissions and the combustion process, mainly because of its influence on the ID. Ladommatos et al. [60] investigated the use of Diesel fuels with CN values ranging from 40.2 to 62.0 by adding ethylhexyl nitrate to the fuel as a CN improver in a co-operative fuel research (CFR) single-cylinder Diesel engine. ***Figure 2-3*** shows the observed relationship between the fuel's CN and the engine's emissions of NO_x (left) and soot (right). Two sets of tests were performed, one with a fixed SOI (FSOI in the figure) and the other with a fixed SOC (FSOC). The left-hand plot shows that NO_x emissions decreased as the fuel's CN increased. This can be attributed to reductions in the peak cylinder temperature and the percentage of fuel burned during the premixed combustion phase as the CN of the fuel increased. Conversely, the right-hand plot shows that soot emissions increased slightly with increasing CN, especially for a fixed SOI. A high CN reduces the extent of premixed combustion and fuel-air mixing, which promotes soot formation. However, it also raises the temperature of the cylinder gas, which favours soot oxidation. These opposing factors may explain the weak dependence of soot emissions on the CN when using the FSOI strategy. HC emissions decreased as the CN increased because long IDs generate overlean fuel-air mixtures

and increase the possibility of wall wetting, leading to increased HC formation. Similar effects on emissions were reported in other studies. [61,62].

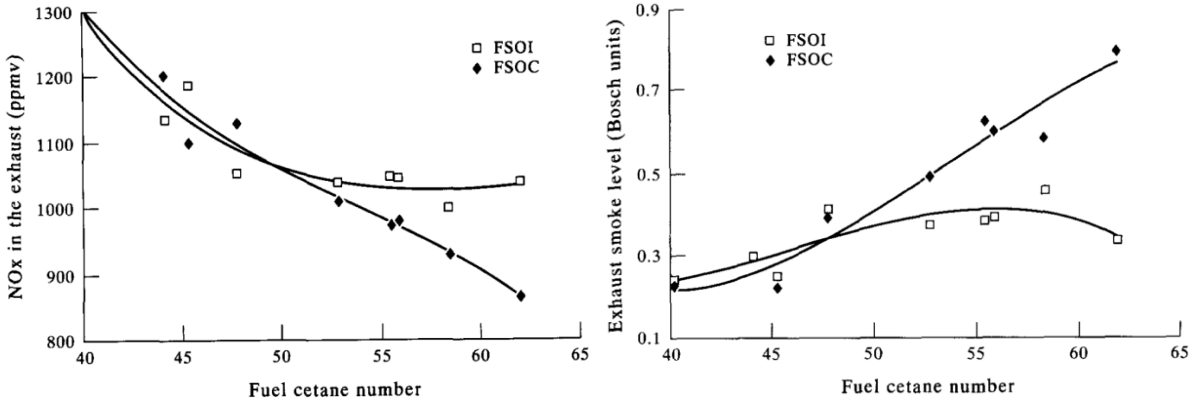

Figure 2-3 Relation between fuel CN and NO (left) and soot (right) emissions [60]

The injection pressure may also influence the relationship between CN and emissions.[63] At high injection pressures, soot emissions are less sensitive to variation in CN. Conversely, NO_x emissions decline with increasing CN regardless of injection pressure. Lü et al. [64,65] studied the influence of CN improvers on emissions from a four-cylinder DI Diesel engine fuelled with ethanol/Diesel blends. Adding a CN improver to the blends partly counteracted their tendency to generate higher CO and HC emissions by reducing the ID, resulting in more complete combustion. Adding a CN improver to the blends further reduced NO_x emissions while only slightly increasing soot emissions. Moreover, the brake thermal efficiency increased with the content of the CN improver in the fuel. İçıngür et al. [66] also reported that adjusting the fuel's CN is an effective way to improve combustion by reducing the ID.

2.4.2 CN measurement

A fuel's CN can be determined using a CFR engine, an ignition quality tester (IQT) [67], a near infra-red (NIR) analyser, or by calculating the cetane index.

The CFR engine method is based on standard D613 of the American Society for Testing and Materials (ASTM). This is the only direct way of measuring a fuel's CN and therefore serves as a reference for all other methods. The CFR cetane rating engine is a single-cylinder continuously variable compression ratio engine. ***Figure 2-4*** shows a schematic of this engine's combustion chamber. The combustion chamber is connected to a swirl chamber. On one side of the swirl chamber, there is a movable plug, which is used to adjust the compression ratio by changing the volume of the combustion chamber. On the other side of the swirl chamber, a standard injector with a pintle-type nozzle is mounted.

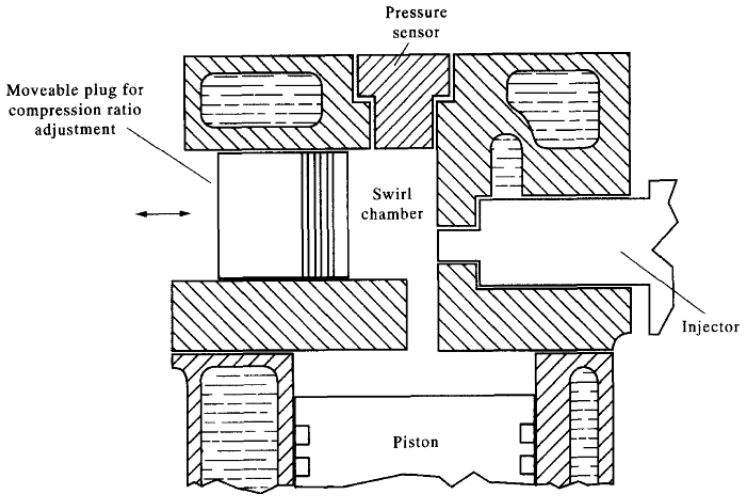

Figure 2-4 Combustion chamber of a CFR engine [60]

The CN scale is defined by two reference fuels: the long straight-chain hydrocarbon hexadecane ($C_{16}H_{34}$), which has good ignition quality and is assigned a CN of 100, and the highly branched compound 2,2,4,4,6,8,8,-heptamethylnonane (HMN, also $C_{16}H_{34}$), which has poor ignition quality and is assigned a CN of 15. [68] If a sample fuel has the same ID as a mixture of these primary reference fuels at a given compression ratio, its CN can be calculated from the volumetric percentages of the two components of the reference fuel as follows:

$$CN = P_{hex} + 0.15 \cdot P_{HMN} \qquad (2.1)$$

where P_{hex} and P_{HMN} are respectively the reference fuel mixture's contents of hexadecane and HMN, expressed as percentages. The CN measurement range of the CFR engine is around 20 to 75.

Methods employing an IQT and fuel ignition testing (FIT) use constant volume combustion apparatus to measure the ID under specific conditions according to ASTM standards D6890 and D7170, respectively. A small amount of specimen fuel is injected into a constant volume combustion chamber with a controlled temperature and pressure, as stipulated by the ASTM standards. After each injection, a pressure curve is recorded, from which the ID can be measured. The measured ID is then used to calculate the derived cetane number (DCN) according to ASTM D6890: [69]

$$DCN = 4.460 + \frac{186.6}{ID} \qquad (2.2)$$

for 3.1 ms ≤ ID ≤ 6.5 ms, or

$$DCN = 83.99 \cdot (ID - 1.512)^{-0.658} + 3.547 \qquad (2.3)$$

for ID < 3.1 ms or ID > 6.5 ms. The measurement should be repeated several times and the average over the repeats should be reported as the final result.

Figure 2-5 shows the precision of different CN measurement methods. The repeatability is defined as the maximum measurement difference obtained with identical samples by the same operator with one engine. Reproducibility is defined as the maximum measurement difference obtained with identical samples by different operators with different equipment. Both the repeatability and reproducibility increase with CN. The IQT method (D6890) has similar repeatability to the CFR engine method (D613) but much lower reproducibility, especially at high CN values.

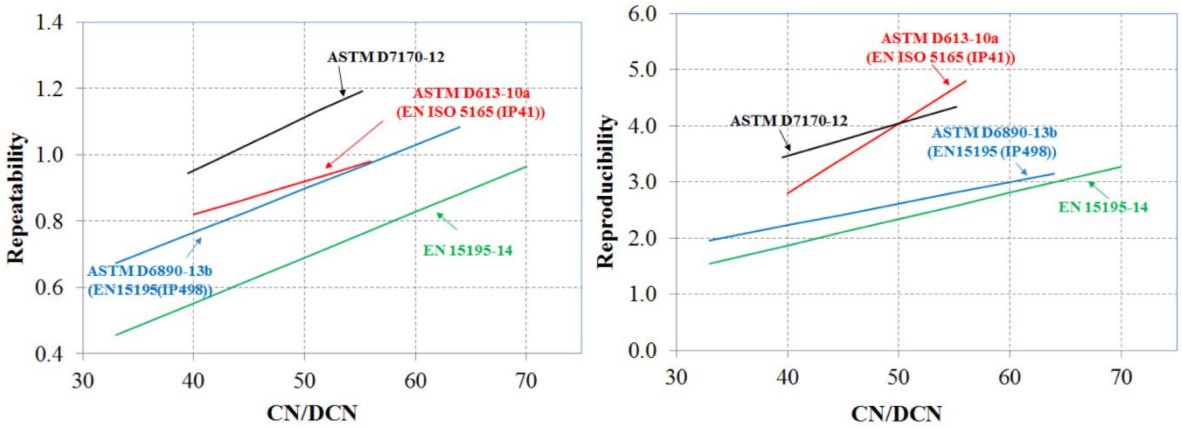

Figure 2-5 Results of repeatability and reproducibility tests performed for different CN/DCN methods [70]

Figure 2-6 compares DCN and CN values obtained by testing 31 fuels representative of commercially available Diesel fuels from North American and European sources and 4 research or specialty fuels. The results confirm that the DCN can be used to predict fuels' CNs; the standard error of prediction is 1.84.

A NIR analyzer can also be used to measure the CN by detecting the absorption spectrum of the target fuel according to ASTM D6122. This is an efficient method for predicting the CN because 10 - 15 measurements can be made in only a few minutes.

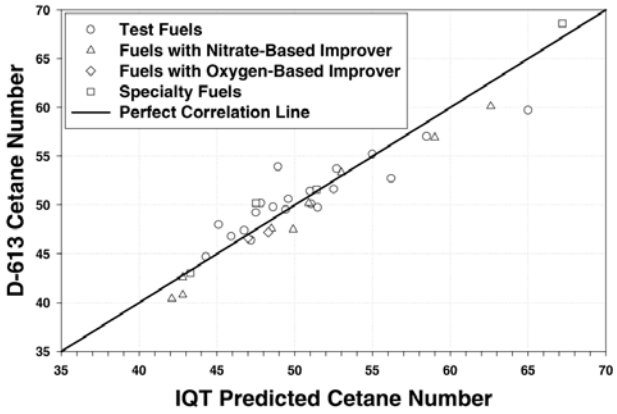

Figure 2-6 Comparison of DCN (IQT) and CN (D-613) values obtained in 35 fuel tests [71]

Numerous cetane index equations have been developed to estimate a fuel's CN from its density and a distillation factor, avoiding the time and expense of conducting an experiment. The ASTM D976 standard includes the following two-variable equation for the cetane index: [72]

$$CI_2 = 454.74 - 1641.416 \cdot \rho + 774.74 \cdot \rho^2 - 0.554 \cdot T_{50} + 97.803 \log^2(T_{50}) \quad (2.4)$$

where ρ is the sample fuel density in g/L at 15 °C and T_{50} is the temperature at which 50 % (v/v) of the sample has evaporated (in °C). An alternative four-variable equation is provided in the ASTM D975 standard: [73]

$$\begin{aligned} CI_4 = {} & 45.2 + 0.0892 \cdot (T_{10} - 215) + (0.131 + 0.901 \cdot B_N)(T_{50} - 260) \\ & + (0.0523 - 0.42 \cdot B_N)(T_{90} - 310) + 0.00049 \cdot [(T_{10} - 215)^2 \\ & - (T_{90} - 310)^2] + 107 \cdot B_N + 60 \cdot {B_N}^2 \end{aligned} \quad (2.5)$$

where $B_N = e^{-3.5(d-0.85)} - 1$ and T_{10}, T_{50} and T_{90} are the temperatures at which 10 vol.%, 50 vol.%, and 90 vol.% of the fuel sample evaporates, in °C.

Figure 2-7 compares calculated cetane index and measured CN values. Although the cetane index does not follow the CN as closely as the DCN, it can still be used to roughly predict trends in CN. Moreover, the 4-variable equation is clearly more accurate than the 2-variable equation especially when the CN is below 55.

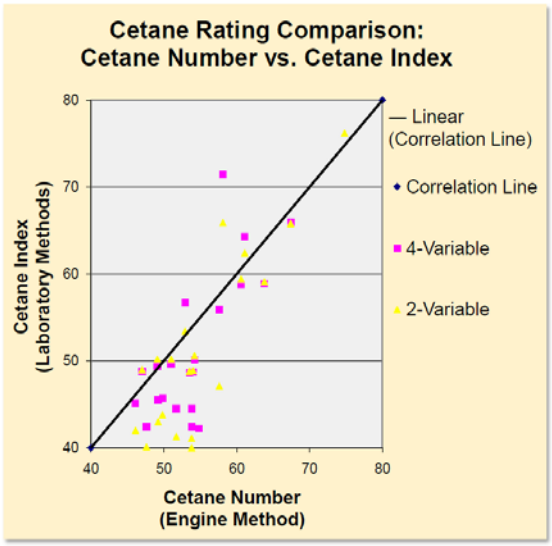

Figure 2-7 Comparison of cetane index and cetane number (CFR) [74]

3 Experimental apparatus and methodology

3.1 Tested fuels

Fossil Diesel, *n*-butanol, isobutanol, 2-ethylhexanol, *n*-octanol, HVO, and RME were used as the main components in the fuel mixtures. The tested Diesel fuel was a winter-type fuel, meeting the EN590 standard but containing no biofuel, FAME. The Diesel fuel was used as one component of some blends and the reference fuel in this study. Tested HVO is so called NExBTL produced by Neste, having similar properties to Diesel fuel but higher CN. RME is a popular biofuel in the Swedish market, being produced from rapeseed oil esterification process. As a FAME fuel, RME shows very good lubricity property [75] and high oxygen content. The tested alcohols were supplied by Perstorp AB in Sweden. N-butanol and isobutanol have higher oxygen content and latent heat of evaporation and lower heating value, viscosity, flash point and boiling point than fossil Diesel, see ***Table 2-1***. As the carbon chain of alcohols increase, *n*-octanol and 2-ethylhexanol, exhibit higher CN, heating value, flash point, and viscosity, and lower oxygen content than shorter carbon chain alcohols, butanol isomers. These make the physical properties of *n*-octanol and 2-ethylhexanol close to the fossil Diesel.

To meet a certain requirement, some additives were added to the tested fuels. DTBP, $(CH_3)_3COOC(CH_3)_3$, is a widely used ignition improver that increases a blend's CN even when added in very small volumes [76]. DTBP was added to some mixtures to compensate for the low CN of alcohols. The DTBP used in the project was called Trigonox B, produced by Akzo Nobel. As a lubricity additive, 200 ppm (by weight) PC32 from Total was added to the blends containing butanol isomers or HVO, because of their poorer lubricity than specified by EN590.

Table 3-1 shows the CN of the selected components (superscript L denotes that the blends were tested in a single-cylinder LD engine, H stands for a single-cylinder HD engine, ML stands for a multi-cylinder engine, and S stands for spray chamber tests). In the table, blends are named using the abbreviations nBu (*n*-butanol), iBu (isobutanol), nOc (*n*-octanol), 2EH (2-ethylhexanol), H (HVO), R (RME), and dtbp (DTBP). The proportion of each component in a given blend by volume is indicated by the number following its abbreviation. The CN of the different blends was determined using a CFR engine complying with the ASTM D-613 standard.

Fossil Diesel was used as reference fuel during the whole tests. Except Diesel, all tested fuels in ***Table 3-1*** was split into three parts. The fuels in the two upper parts, alcohol/Diesel blends and fossil-free fuels, appear the similar CN to Diesel (52), except HVO. Therefore, no engine

modification is needed when replacing Diesel fuel by the fuels. As alcohol/Diesel blends, blends with 10 and 20 % butanol isomers were selected for two main reasons. Firstly, the blends' high percentage of butanol was expected to have a strong influence on the combustion characteristics and emissions. When butanol isomers are mixed in Diesel at levels higher than 30 %, NO_x emissions and fuel consumption have been shown to increase, whereas the maximum brake power and maximum torque may decrease. [77] Secondly, as can be seen from the data in ***Table 3-1***, the effect of DTBP in increasing the CN seems to be close to its limit for the blends nBu20D and isoBu20D, and therefore it may not have been possible to raise the CN of a blend with 30 % isobutanol to ~52. Therefore, the selected blends were seen as a good compromise.

Table 3-1 CN of the tested fuels

	Blends	Diesel Vol.%	*n*-Butanol Vol.%	Isobutanol Vol.%	2-Ethylhexanol Vol.%	*n*-Octanol Vol.%	HVO Vol.%	RME Vol. %	DTBP mg/kg	CN -
	Diesel ^{L,H,ML,S}	100	-	-	-	-	-	-	-	52
Alcohol/Diesel blends	nBu10H20D70 ^{L,H}	70	10	-	-	-	20	-	-	50.6
	nBu10D90dtbp ^{L,H}	90	10	-	-	-	-	-	600	51.3
	nBu20H40D40 ^{L,H,ML,S}	40	20	-	-	-	40	-	-	50.3
	nBu20D80dtbp ^{L,H,S}	80	20	-	-	-	-	-	12000	~49.0
	isoBu10H30D60 ^{H}	60	-	10	-	-	30	-	-	51.7
	isoBu20H60D20 ^{L,H}	20	-	20	-	-	60	-	-	52.5
	isoBu20D80dtbp ^{L,H}	80	-	20	-	-	-	-	12000	49.0
	2EH30D70dtbp ^{L,H}	70	-	-	30	-	-	-	6000	49.9
	2EH30H40D30 ^{L,ML}	30	-	-	30	-	40	-	-	51.3
	nOc30H20D50 ^{L}	50	-	-	-	30	20	-	-	53.1
	nOc30D70dtbp ^{H,L}	70	-	-	-	30	-	-	800	50.8
Fossil-free fuels	nBu30H70 ^{L,H,S}	-	30	-	-	-	70	-	-	51.1
	nBu28HR7H ^{L,H}	-	28	-	-	-	65	7	-	50.6
	nOc55H ^{L,H}	-	-	-	-	55	45	-	-	51.7
	nOc51R7H ^{L,H}	-	-	-	-	51	42	7	-	51.7
	2EH40H ^{L,H}	-	-	-	40	-	60	-	-	51.3
	2EH37R7H ^{L,H}	-	-	-	37	-	56	7	-	51.3
	2EH30R25H45 ^{H}	-	-	-	-	-	-	-	-	51.2
	HVO ^{S}	-	-	-	-	-	100	-	-	75.1
	RME ^{H}	-	-	-	-	-	-	100	-	53.4
Low CN fuels	nBu100 ^{S}	-	100	-	-	-	-	-	-	<20
	nBu20D80 ^{S}	80	20	-	-	-	-	-	-	39.1
	nBu30D70 ^{L,S}	70	30	-	-	-	-	-	-	35.2
	nBu60D40 ^{L,H}	40	60	-	-	-	-	-	-	25.8
	iBu50D50 ^{L}	50	-	50	-	-	-	-	-	25.2
	nOc100 ^{L,S}	-	-	-	-	100	-	-	-	37.5

^{L} denotes LD engine tests, ^{H} denotes HD engine tests, ^{ML} denotes multi-cylinder LD engine tests, and ^{S} denotes spray chamber tests.

Fuels in the bottom part, low CN fuels, in ***Table 3-1*** appear lower CN than fossil Diesel to achieve PPC. To find the best candidates, a lot of CNs of Diesel/alcohol blends were measured in a CFR engine. ***Figure 3-1*** shows the CNs as functions of blends' alcohol content. As the

blends' alcohol content increases, their CN decreases. CNs below 20 could not be measured reliably with our apparatus, so values for neat *n*-butanol and isobutanol were estimated based on the literature [78]; this is indicated by the use of dashed lines in the figure. The CNs of the alcohol/Diesel blends featuring the longer-chained octanol isomers vary more linearly with the alcohol content than do those for the butanol/Diesel mixtures.

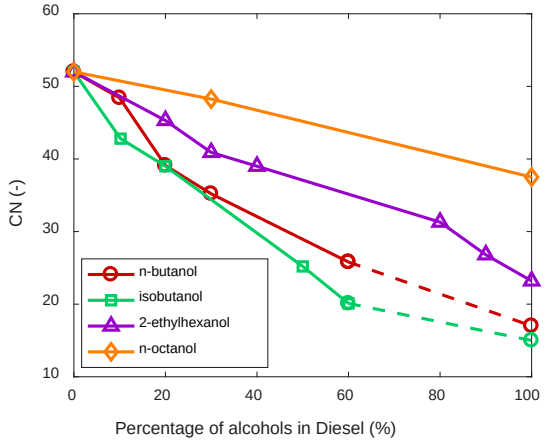

Figure 3-1 CN values for different alcohol/Diesel blends as functions of their alcohol content.

Partially premixed combustion experiments were conducted with fuels having two different CN levels, see the bottom part of ***Table 3-1*** except nBu100. Fuels with a CN of 26 (nBu60, iBu50, and 2EH90) were tested because nBu60 achieved promisingly high thermal efficiencies in HD engine experiments [79]. Fuels with a CN of 36 (nOct100 and nBu30) were tested as intermediates between the high and low CN extremes represented by neat Diesel and nBu60.

Diesel fuel was used as a reference fuel in every test, conventional CI combustion, fossil-free fuels conventional CI combustion, partially premixed combustion, and constant volume combustion chamber tests. HVO and nBu100 were only tested in the spray chamber due to their extremely high and low CN.

3.2 Tested engines

To investigate the effects of using alcohols in Diesel fuel, three types of engines were used. A single cylinder LD engine and a single cylinder HD engine were utilized to study the effect of using Diesel and alcohol blends on performance and emissions in conventional CI combustion and partially premixed combustion. In addition, a four-cylinder LD engine was applied to study the cold start behaviour when using alcohol/Diesel blends.

3.2.1 HD engine specifications and operating conditions

A 2 litre AVL 501 single cylinder HD Diesel engine was employed for alcohol/Diesel blends conventional CI combustion, which was equipped with a common rail injection system and a cylinder head and piston based on the Volvo Powertrain D12C engine. ***Table 3-2*** shows the engine's specifications. The test engine used a Delphi F2 distributed pump Diesel common rail system, which enabled the use of higher (up to 270 MPa) and more stable injection pressures.

Table 3-2 Specifications of the single-cylinder HD engine for alcohol/Diesel blends conventional CI combustion

Engine type	AVL 501 Single cylinder
Bore	131 mm
Stroke	150 mm
Valves	4
Connecting rod length	260 mm
Compression ratio	17:1
Piston head geometry	Omega shaped
Fuel injection system	Common rail
Injection pressure	180 MPa
Nozzle	5 holes

A 2.2 litre AVL 501 single cylinder HD engine Diesel engine was used for fossil-free fuels conventional CI combustion and the partially premixed combustion. ***Table 3-3*** shows the engine's specifications. The HD engine was equipped with a Volvo Powertrain D13 cylinder head and a common rail injection system.

Table 3-3 Specifications of the single-cylinder HD engine for fossil-free fuels conventional CI combustion and the partially premixed combustion

Engine type	AVL 501 Single cylinder
Bore	131 mm
Stroke	158 mm
Valves	4
Connecting rod length	260 mm
Compression ratio	17:1
Piston head geometry	Wave, omega shaped
Nozzle	6 holes
Fuel injection system	Common rail

To investigate the effect of piston bowl geometry on engine performance and emissions, a Volvo prototype 6-wave piston, and a standard ω-bowl piston were utilized, see ***Figure 3-2***. The so called wave piston [80] has the same compression ratio of 17:1 as the standard piston. A

6-hole nozzle fit the wave piston very well that each fuel jet is injected into the centre of the 'wave trough'. The same injector was applied in both pistons experiments.

(a) (b)

Figure 3-2 The geometries of the tested a) 6-wave piston and b) standard ω-bowl piston.

Figure 3-3 shows a schematic of the HD engine test bed for conventional CI combustion and partially premixed combustion. An AVL 733S fuel balance was used to measure the fuel mass flow rate with the accuracy 0.12 - 0.16 % of measurements, and the fuel was passed through a conditioning unit before delivery to the pumping injector. A Kistler 7061B pressure sensor, a Kistler 3066A01 piezo amplifier and an Osiris data acquisition system were used to acquire cylinder pressure data at 0.1 crank angle degrees (CAD) resolution for 100 cycles. To correct the cylinder pressure measurement, Osiris recorded the high frequency intake temperature and intake pressure signal as well. The EGR was adjusted by controlling the backpressure with a valve placed in the exhaust pipe. The recirculated exhaust gases were cooled by a water cooler before being mixed with the compressed intake air, whose humidity and temperature were measured. LabView was applied to communicate with engine control unit (ECU) to control the injection. AVL Puma system acquired all the low frequency signals from thermal couples, pressure transducers, fuel balance, and emission analysers.

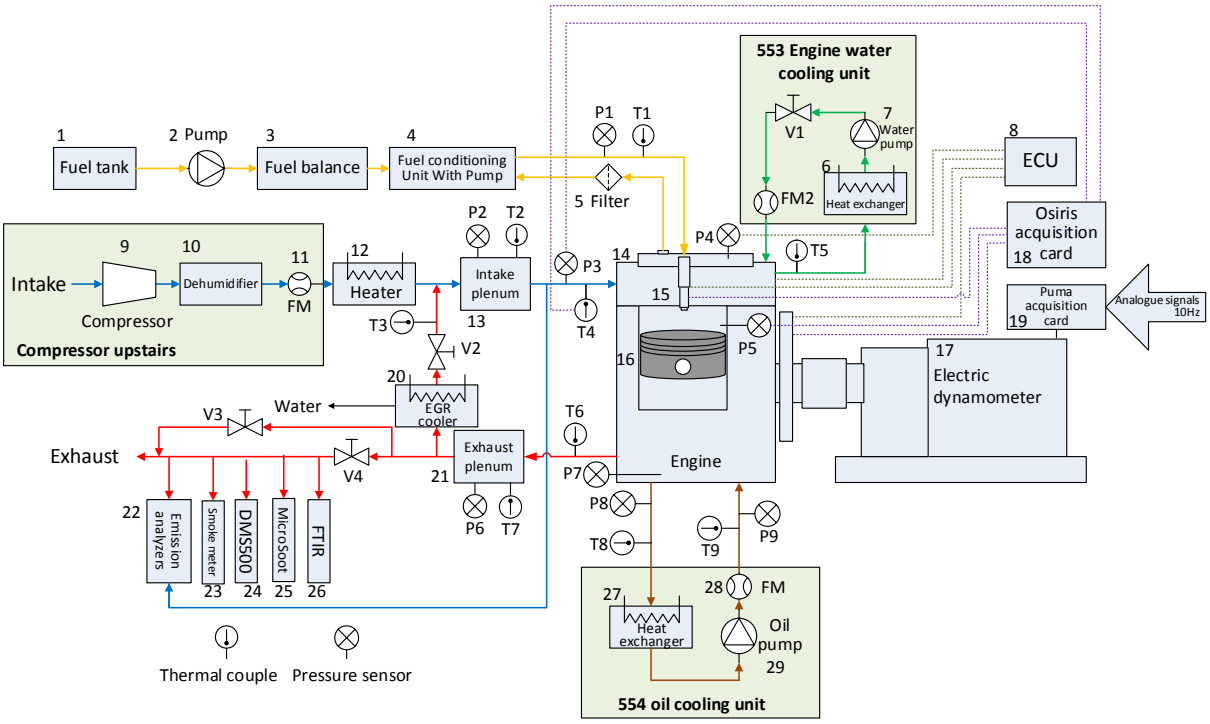

Figure 3-3 Schematic of the HD engine experimental setup

The concentrations of HC, nitric oxide (NO), carbon monoxide (CO), CO_2, oxygen (O_2), formaldehyde, and particulate matter size distribution in the exhaust gases were measured. The emission analyzers and their accuracy are shown in ***Table 3-4***.

Table 3-4 Measuring equipment for the HD engine setup

	Equipment	Accuracy
HC	CUTTER FID i60 LHD	< 0.5 % of full scale
NO_x	CLD i60 HHD SLQ	< 0.5 % of full scale
CO high	IRD i60 H	< 0.5 % of full scale
CO low	IRD i60 L	< 0.5 % of full scale
CO_2 inlet	IRD i60 L	< 0.5 % of full scale
CO_2 exhaust	IRD i60 H	< 0.5 % of full scale
O_2	PMD i60	< 0.5 % of full scale
Soot	AVL Micro soot sensor	< 0.01 mg/m^3
PM distribution	Particulate spectrometer CombustionDMS500	< 5 % in general
Formaldehyde	FT-IR	2 %
Fuel consumption	AVL 733S fuel balance	0.12 - 0.16 %

Figure 3-4 shows the operating conditions of the HD Diesel engine for all conventional CI combustion. Four operating points from the European Stationary Cycle were chosen: A25, B50, C75, and B75. B50 was chosen as the reference point.

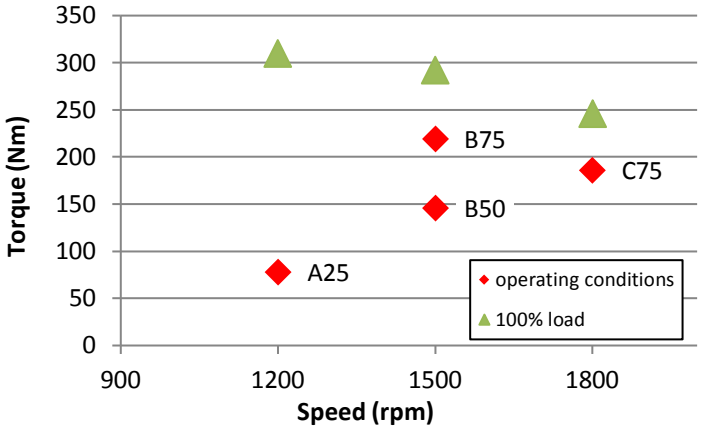

Figure 3-4 Operating conditions of the HD engine

3.2.2 LD engine specifications and conditions

Single cylinder LD engine tests were conducted in a Ricardo Hydra engine equipped with a Volvo VED4 cylinder head and a common rail injection system. ***Table 3-5*** shows the engine's specifications.

Table 3-5 Specifications of the single-cylinder LD engine

Engine type	Ricardo Hydra engine
Bore	82 mm
Stroke	93 mm
Compression ratio	15.8:1
Fuel injection system	Common rail

Figure 3-5 shows a schematic of the LD engine test bed. Fuel mass flow was measured by an AVL 730 fuel balance. A Denso injector was used to generate up to 4 pulse injections per cycle. An AVL GU12S-10 pressure transducer was installed to measure the in-cylinder pressure based on a charge difference. The change in signal was amplified by a Kistler 5011 piezo amplifier and acquired by an AVL IndiCom system. Alone with cylinder pressure, injection current, and injection pressure were processed by IndiCom. The crank angle resolution of the cylinder pressure was 0.2 CAD. An INCA system was used to communicate with ECU and control the injection strategy and swirl ratio. Sense tool recorded the low frequency signal from thermal couples, pressure transducers, and emissions analyzers.

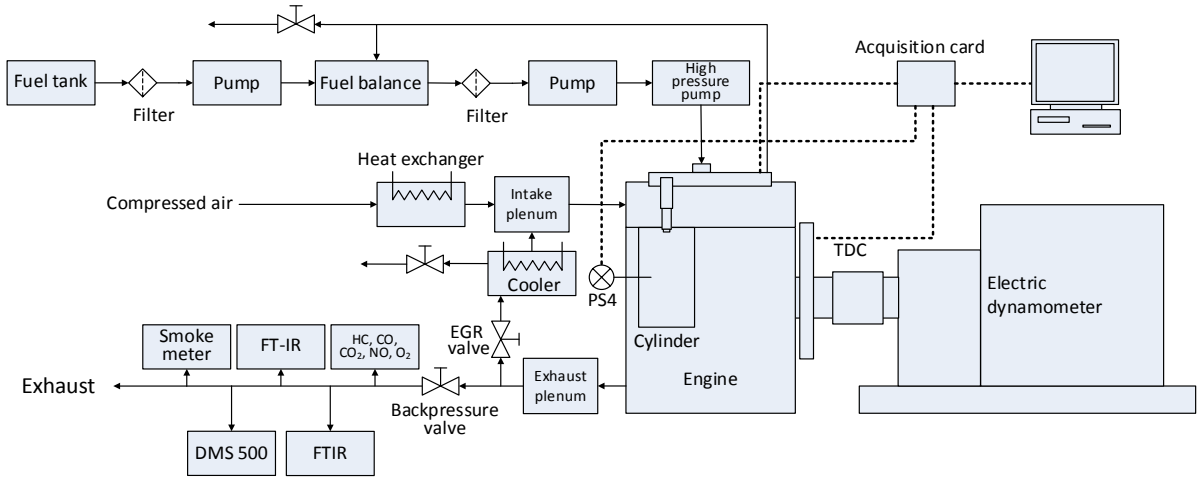

Figure 3-5 Schematic of the LD engine experimental setup

In the LD engine tests, regular emissions, particulate matter size distribution and fuel consumption were measured by the equipment shown in ***Table 3-6***, along with their accuracy.

Table 3-6 Measuring equipment for the LD engine setup

	Equipment	Accuracy
HC	JUM model 3-300 FID	-
NO_x	Rosemount CLD 951A	< 0.5 % of full scale
CO	Rosemount Binos 1001/1004	< 2 % of full scale
CO_2 inlet	Rosemount Binos 1001/1004	< 2 % of full scale
CO_2 exhaust	Rosemount Binos 1001/1004	< 2 % of full scale
Soot	AVL Micro soot sensor	< 0.01 mg/m^3
PM distribution	Particulate spectrometer Combustion DMS500	< 5 % in general
Fuel consumption	AVL 733S fuel balance	0.40 - 1.52 %

During particulate size distribution measurements, to maintain a good signal-to-noise ratio, the second stage of dilution was adjusted when changing the operating conditions, but it was not adjusted when changing fuels.

For conventional CI combustion, four different operating points were chosen based on the New European Driving Cycle, 1) 5 Nm, 1200 rpm, 2) 30 Nm, 1280 rpm, 3) 23 Nm, 1810 rpm, and 4) 36 Nm, 2000 rpm. All the blends were tested under the same engine settings. A multi-injection strategy and EGR were applied in these tests. Swirl management was employed to adjust the swirl ratio to match the various engine loads.

3.2.3 Multi-cylinder engine specifications and conditions

A four cylinder Volvo Car's VED4 engine equipped with a high performance (HP) turbo system and common rail system was used for the cold start tests. ***Table 3-7*** shows the engine specifications. The tests were conducted in Volvo Cars cold start engine test facilities with a set-up close to vehicle conditions. Prior to the tests, the engine was cooled to 2 °C below the target starting temperature. The temperature was then adjusted to the starting temperature and kept constant for 2 hours. The engine was cooled using the cooling equipment of the room and cooling fans directed at the engine.

Table 3-7 Specifications of the multi-cylinder LD engine

Engine type	VED4 HP
Bore	82 mm
Stroke	93.2 mm
Displacement	1.9691
Compression ratio	15.8:1
Fuel injection system	Common rail, 7 holes injector
Injection pressure	Approx. 45 MPa at start, 20-180 MPa during run
Firing order	1,3,4,2
Glow plug tip temp	1250 °C

After performing a cold start, data were collected for 120 seconds at idling. The engine was subsequently run at 2200 rpm until the cooling water temperature reached 80 °C. Afterwards, the engine was shut down and another cooling sequence was initiated. Three fuels were tested: Diesel fuel, nBu20H and 2EH30H. Each of the fuels was tested three times at each studied temperature, i.e. 0, -10,-20, -25 and -30 °C.

3.3 Constant volume combustion chamber

Figure 3-6 shows the schematic of an optically-accessible high pressure high temperature constant volume combustion chamber experimental setup. A continuous-gas-flow was generated by a compressor and heated by two 15 kW heaters before entering the chamber. The velocity of the air was restricted below 0.1 m/s in the combustion chamber. Because the magnitude of air flow was much smaller than the velocity of fuel jet (over 100 m/s), the ambient air condition could be considered quiescent.

The maximum steady-state temperatures and pressure achievable with this system are 900 K and 10 MPa, respectively. A fuel injector was mounted at the center of the bottom face of the chamber, injecting the fuel directly upwards. The injector was fitted with a straight single-hole nozzle with a diameter of 0.19 mm. The tested fuels were pressurized using a Scania XPI common rail fuel supply system.

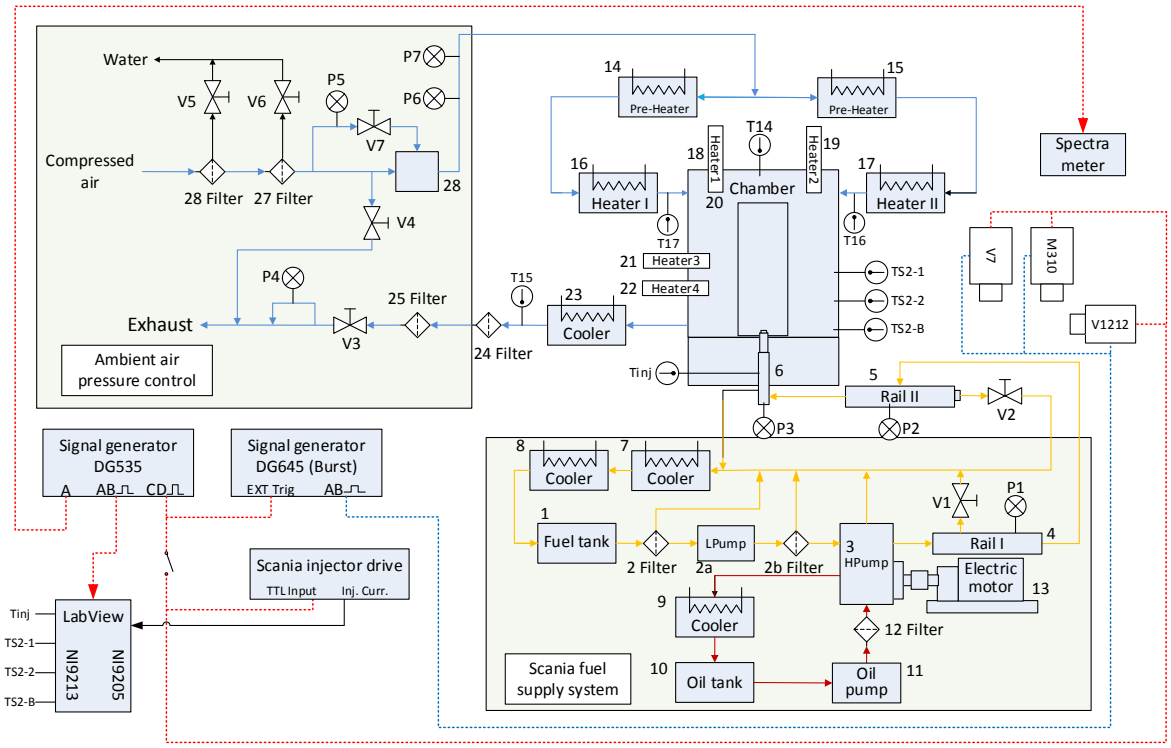

Figure 3-6 Schematic of the high pressure high temperature constant volume combustion chamber experimental setup

Back-illumination imaging was used to characterize the liquid and vapour phase sprays under non-combusting conditions. A schematic of the optical setup is shown in ***Figure 3-7***. A diffuse screen (DF) was placed between the halogen lamps and the spray chamber to generate homogeneous light. To increase the optical sensitivity of the refractive index gradients at vapor air boundary, the diffuse screen was replaced by the one with black strips. Spray penetration images were captured with a Phantom V1212 high-speed video CMOS camera.

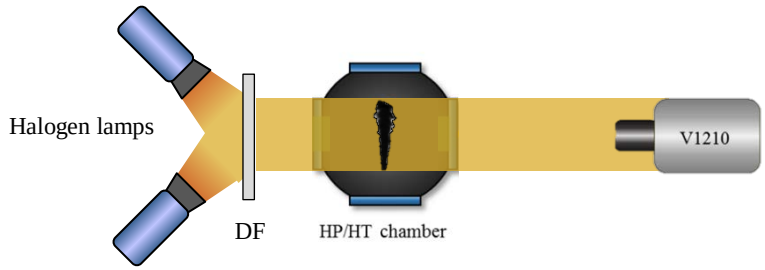

Figure 3-7 Optical set-up with the constant volume combustion chamber for non-combusting conditions

Figure 3-8 shows the optical set-up for simultaneous high-speed visualization of the combustion chamber under combusting conditions. A continuous wave Nd:YAG 532 nm laser was used as the light source when recording soot extinction images using a bandpass filter (BF2 532 ± 1.5 nm) and V1212 high-speed camera. **A** bandpass filter (BF1 307 ± 5 nm) was used to enable recording of UV light to quantify OH* chemiluminescence by a high-speed camera V7. The natural flame luminescence images were captured by a long pass filter (LF OG570) and M310 high-speed camera**.** All cameras were synchronized using a Stanford Research Systems signal generator and had a frame rate of 27,777/s. The setup of the combustion chamber and the optical system is described in greater detail elsewhere [81,82].

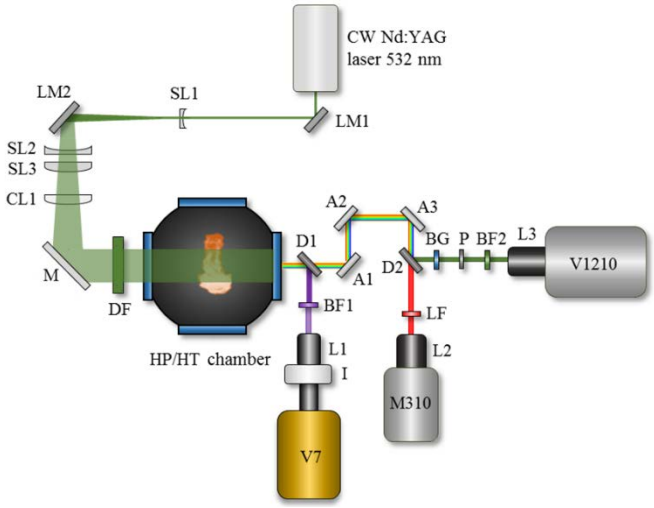

Figure 3-8 Optical set-up of the constant volume combustion chamber for combusting conditions [82]

Two test conditions were applied in this work, non-combusting and combusting (see ***Table 3-8***). In addition, two injection pressures were studied: 120 MPa and 180 MPa. The ambient temperature was set to 623 K or 823 K to establish non-combusting and combusting conditions, respectively. An ambient air density of 26 kg/m^3 was selected to mimic practical low-load operating conditions (n = 1200 rpm, IMEP = 0.59 MPa) for a heavy-duty engine [83]. Thirty measurements were acquired at each operating point, enabling computation of average values and standard deviations.

Table 3-8 Experimental operating conditions

	non-Comb condition	Comb condition
Injection pressure, MPa	120, 180	120, 180
Injection duration, ms	1.7	3
Ambient temperature, K	623	823
Ambient pressure, MPa	4.59	6.04
Ambient density, kg/m3	26	26

3.4 Data evaluation

3.4.1 Heat release rate

The rate of heat release was calculated based on the cylinder pressure. Generally, the heat release rate was calculated using the first law of thermodynamics:

$$\delta Q_{release} = dU + \delta Q_{transfer} + \delta W \tag{3.1}$$

where U is the internal energy of the cylinder contents, Q_{transfer} is the heat transfer to the chamber walls and W is the work done on the piston. If it is assumed that the contents of the cylinder can be modelled as an ideal gas, dU is given by

$$dU = \frac{c_v}{r} pdV + \frac{c_v}{r} Vdp \tag{3.2}$$

where p is the cylinder pressure and V is the volume of the combustion chamber, the specific gas constant r is calculated by the ideal gas constant R = 8.314 J/mol·K,

$$r = \frac{R}{M} \tag{3.3}$$

M is the average molar mass of the gas mixture, c_{v} is the specific heat capacity at constant volume, which can be calculated as below:

$$c_v = c_p - r \tag{3.4}$$

where c_p is the specific heat capacity at constant pressure. Heat capacity ratio γ is:

$$\gamma = \frac{c_p}{c_v} \tag{3.5}$$

Substitute the ***Equation 3.5*** and ***Equation 3.4*** into ***Equation 3.2***, the simplified dU is:

$$dU = \frac{1}{\gamma - 1}(pdV + Vdp) \tag{3.6}$$

For a fast calculation, a constant $\gamma = 1.3$ [90] was used during a whole combustion process. Practically, however, γ changes as cylinder temperature. For a more accurate heat release rate, specific constant pressure heat per mole c_p of each gas component can be calculated by:

$$\tilde{c}_{p,i} = (a_1 + a_2 T + a_3 T^2 + a_4 T^3 + a_5 T^4) \cdot R \tag{3.7}$$

Then the specific constant pressure heat capacity of mixture $c_{p,mixture}$ is as below:

$$c_{p,mixture} = \frac{\sum(\tilde{c}_{p,i} \cdot n_i)}{m_{mixture}} \tag{3.8}$$

The heat transfer between the cylinder contents and chamber wall can be defined as follows:

$$Q_{transfer} = hA(T - T_w) \tag{3.9}$$

where *h* is the heat transfer coefficient, *A* is the exposed combustion chamber surface area, *T* is the temperature of the cylinder gas and T_w is the cylinder wall temperature. The Woschni heat transfer coefficient [84] can be expressed as

$$h = 3.26 \cdot B^{-0.2} \cdot p^{0.8} \cdot T^{-0.55} \cdot w^{0.8} \tag{3.10}$$

where *B* is the cylinder diameter, *T* is the cylinder pressure and *w* is the average cylinder gas velocity, which is calculated as below [90]:

$$w = 2.28 \cdot \bar{S}_P + 0.00324 \cdot \frac{V_d \cdot T_{ivc}}{p_{ivc} \cdot V_{ivc}} \cdot (p - p_m) \tag{3.11}$$

where $\bar{S}_P$ is mean piston speed, is the displacement volume, T_{ivc}, p_{ivc}, and V_{ivc} are the temperature, pressure and volume at the inlet valve closing (IVC), and p_m is the motored cylinder pressure at the same crank angle as p.

δW was calculated as below:

$$\delta W = pdV \tag{3.12}$$

3.4.2 Evaluation related to changing fuel

The LHV is an important property of a fuel because it influences the combustion behaviour and emissions. For a blend comprising Diesel fuel, alcohol, and an ignition improver, LHV depends on the proportions of the individual components, as shown below:

$$LHV_{blend} = \sum_{i}^{n} V_i \cdot \rho_i \cdot LHV_i \qquad (3.13)$$

where V_i, ρ_i and LHV_i are the volume percentage, density and LHV of component i, respectively.

When changing Diesel fuel to blends, the different hydrogen, nitrogen and oxygen content and density of HC will influence the specific emissions. Therefore, factors in equations need to be determined for specific emissions.

Gas emissions from exhaust gases are normally measured in parts per million (ppm) by volume (soot emissions are converted to mg/kg). To make emissions data more comparable, they need to be converted to specific values. Specific emissions of soot, HC, CO_2, CO, and NO_x, can be derived according to the following equation:

$$e = \frac{q_c \times 3.6}{P} \qquad (3.14)$$

Where q_c is the emission component mass flow rate in mg/s and P is the power in kW. The soot mass flow rate in the exhaust can be calculated as below:

$$q_{Soot} = \frac{1}{0.405} \times 4.95 \cdot FSN \cdot e^{0.38 \times FSN} \times \frac{1}{1.169} \cdot (q_{mf} + q_{mair}) \qquad (3.15)$$

For HCs, CO_2, CO and NO_x, the emission component mass flow rate is

$$q_c = \frac{\rho_c}{\rho_e} \cdot c \cdot (q_{mf} + q_{mair}) \qquad (3.16)$$

Where ρ_c is the density of one exhaust gas component in kg/m^3, ρ_e is the density of the exhaust gas in kg/m^3, c is the one component concentration in ppm, q_c is the emission component mass flow rate in mg/s, q_{mf} is the instantaneous fuel mass flow rate in kg/s and q_{mair} is the instantaneous dry intake air mass flow rate in kg/s, which is calculated using Spindt method shown later.

In addition, the density of the exhaust gas can be derived as follows [85, 86]:

$$\rho_e = \frac{1000 + H_a + 1000 \times \frac{q_{mf}}{q_{mair}}}{773.4 + 1.2442 \times H_a + k_f \times 1000 \times \frac{q_{mf}}{q_{mair}}} \quad (3.17)$$

with

$$k_f = 0.05594 \cdot w_{ALF} + 0.0080021 \cdot w_{DEL} + 0.0070046 \cdot w_{EPS} \quad (3.18)$$

where H_a is the intake air humidity (g water per kg dry air) and w_{ALF}, w_{DEL} and w_{EPS} are the hydrogen, nitrogen and oxygen content of the fuel (in wt.%), respectively.

As mentioned above, CO_2 and CO were measured as dry gas. Therefore, a dry-to-wet correction factor was needed to convert the measured value to a real (wet) value according to the following equation:

$$c_w = k_w \cdot c_d \quad (3.19)$$

where c_d is the dry gas concentration in ppm and k_w is the dry-to-wet correction factor. Under the experimental conditions used in this study, the dry-to-wet correction factor was calculated as follows:

$$k_w = (1 - \frac{1.2442 \times H_a + 111.19 \times w_{ALF} \times \frac{q_{mf}}{q_{mair}}}{773.4 + 1.2442 \times H_a + \frac{q_{mf}}{q_{mair}} \times k_f \times 1000}) \times 1.008 \quad (3.20)$$

The NO_x emission concentration also needed to be corrected using the following equation:

$$c_{corr} = \frac{1}{1 - 0.0182 \cdot (H_a - 10.71) + 0.0045 \cdot (T_{air} - 25)} \cdot c_{NOx} \quad (3.21)$$

where T_{air} is the intake air temperature and c_{NOx} is the measured concentration of NO_x in ppm.

3.4.3 Other calculations

Lambda was measured by a lambda sensor and calculated based on the emissions. To calculate lambda, Spindt method [87] was applied as follows:

$$R = P_{CO}/P_{CO2} \quad (3.22)$$

$$Q = P_{O2}/P_{CO2} \tag{3.23}$$

$$F_b = (P_{CO} + P_{CO2})/(P_{CO} + P_{CO2} + P_{HC}) \tag{3.24}$$

$$\frac{A}{F} = F_b \left[11.492 \times F_C \left(\frac{1 + \frac{R}{2} + Q}{1 + R} \right) + \frac{120(1 - F_C)}{3.5 + R} \right] \tag{3.25}$$

where P_{CO}, P_{CO2}, P_{O2} and P_{HC} is percentage concentractions of CO, CO_2, O_2, and HC in exhaust gases. F_C is carbon fraction in the fuel.

The concentration of CO_2 was measured at both the intake and exhaust system to calculate the EGR ratio as follows:

$$EGR = \frac{CO_{2\,intake} - CO_{2\,air}}{CO_{2\,exhaust} - CO_{2\,air}} \times 100\% \tag{3.26}$$

The start of combustion (SOC) is determined according to the average heat release curve of 100 - 300 cycles, showing the crack angle where the heat release curve cross zero from negative to positive. In the study, the start of injection (SOI), end of injection (EOI) and SOC were used to define the ignition delay, ignition dwell, and combustion duration as below:

$$Ignition\ delay = SOC - SOI$$

$$Ignition\ dwell = SOC - EOI$$

$$Combustion\ duration = CA90 - CA10$$

3.4.4 Statistical analysis

For conventional CI combustion tests, operating condition B50 for the HD engine and point 2 (30 Nm, 1280 rpm) for the LD engine were tested several times for each fuel, especially for Diesel fuel. The repeated tests (3 to 10 times) provide the opportunities to use analysis of variance (ANOVA) tables to check the significance of the variables when comparing alternative fuels to fossil Diesel. The confidence interval was set to 95 %.

Two methods were used to check the repeatability of the results and stability of combustion. Error bars represented the standard deviation of repeated reference measurements made between each change of operating conditions. Thus, the error bars showed the repeatability of the results for a particular fuel and operating condition. In addition, the coefficient of variation (COV) of the IMEP was used to show the cycle-to-cycle variation, as calculated below:

$$COV_{IMEP} = \frac{\sqrt{\frac{1}{n}\sum_i^n (IMEP_i - \overline{IMEP})^2}}{\overline{IMEP}} \times 100\% \quad (3.27)$$

where $IMEP_i$ is the IMEP of individual cycle and $\overline{IMEP}$ is the mean value of IMEP in one measurement.

In spray chamber tests, more than 30 times events were measured for each fuel under each condition, therefore the standard deviation was shown for parameters, such as ignition delay times and flame lift-off length.

3.4.5 Spray image processing

Both of the liquid and vapour phase spray evaluation rely on the measurement of attenuation of light by an absorbing and/or scattering medium, liquid spray, vapour spray and heated air.

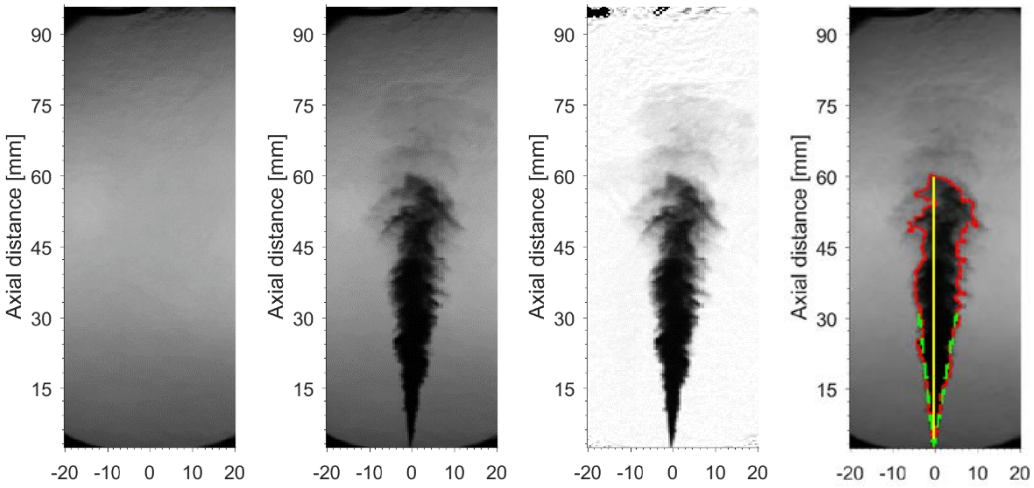

a) Background b) Original image c) Proceed image d) Boundary image

Figure 3-9 Liquid phase spray penetration and spray cone angle processing procedure. Diesel fuel injection at injection pressure of 120 MPa, ambient temperature of 623 K, gas density of 26 kg/m^3 and 2 ms after the electronic start of injection. Red line is liquid phase boundary, yellow line is penetration and green dash lines show the spray cone angle.

Figure 3-9 shows the liquid phase spray penetration and spray cone angle processing procedure. Liquid phase spray boundary, shown as a red line in ***Figure 3-9 d***, was determined by applying a threshold (0.6) on a background subtracted image, see ***Figure 3-9 c***. The liquid penetration is

the longest distance from the needle tip to the farthest boundary point in the central line, shown as a yellow line in ***Figure 3-9 d***. The liquid phase spray cone angle is calculated as below:

$$\theta = 2tan^{-1}\frac{A_{s/2}}{(s/2)^2} \qquad (3.28)$$

where $A_{s/2}$ is the spray area of first half penetration from the nozzle tip, s is the liquid phase penetration.

Figure 3-10 shows the procedure of calculating vapour phase penetration. Vapour penetration was determined from the images with striped background by calculating the difference between consecutive images. This method is more sensitive to refraction by the fast moving jet edge than the slow change of surrounding air movement [81]. The red line in ***Figure 3-10 d*** demonstrates the vapour phase penetration.

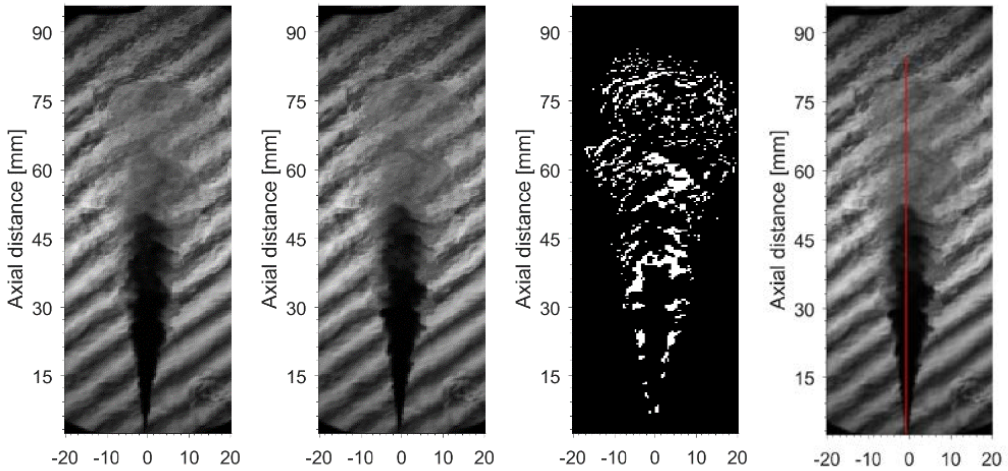

a) I_{n-1} b) I_n c) I_n - I_{n-1} d) Penetration

Figure 3-10 Vapour phase spray penetration processing procedure. Diesel fuel injection at injection pressure of 120 MPa, ambient temperature of 623 K, gas density of 26 kg/m^3 and 2 ms after the electronic start of injection. Red line is vapour phase penetration

The evaluation of the soot and images follow the same procedure as in Ref [82]. According to the Beer–Lambert law, the soot optical thickness, KL, was determined by comparing the transmitted laser intensity, *I*, to the baseline laser intensity, I_0:

$$\frac{I}{I_0} = e^{-KL} \tag{3.29}$$

where K is the dimensional extinction coefficient and L is the path length through the soot cloud. The soot volume fraction, f_V, was determined from the dimensional extinction coefficient data, using expressions derived from Rayleigh–Debye–Gans (RDG) approximation theory:

$$f_V = \frac{K\lambda}{K_e} \tag{3.30}$$

where λ is the laser wavelength and K_e is the dimensionless optical extinction coefficient, which is given by the following equation:

$$K_e = (1 + \alpha_{sa})6\pi E(m) \tag{3.31}$$

where, α_{sa} is the scattering-to-absorption ratio, m is the refractive index of soot, and

$$E(m) = -Im[(m^2 - 1)/(m^2 + 2)] \tag{3.32}$$

for a laser wavelength of 532 nm, $m = 1.61 - i0.74$ [82,88]. Therefore, a value of K_e = 6.1 was selected to relate the KL to the soot volume fraction. The total soot mass was calculated as:

$$M_{soot} = A_p(\rho\lambda/K_e)\sum KL \tag{3.33}$$

where A_p is the area of one pixel and the particle density ρ is 1.8 g/cm^3 [89].

The extinction coefficient data, KL, was averaged over multiple individual images with similar axisymmetric structures. The left and right halves (separated by the jet axis) of the-time averaged KL images were transformed by three-point Abel inversion, allowing the cross-sectional soot volume fraction distribution to be determined by combining the continuous quantitative KL measurements with flame boundaries determined from flame luminosity images. The ignition delay time was defined as the time between the first frame featuring a detectable liquid spray, i.e. the start of injection (SOI), and the time of the first frame in which the light intensity exceeded the background noise in the OH* images, i.e. the SOC. The OH* chemiluminescence images were used to determine the flame LOL.

4 Results and discussion

This chapter discusses the effects of using alcohols and alcohol blends on combustion behaviour and emissions as observed in the constant volume combustion chamber and internal combustion engine experiments conducted within this project. The major findings of the attached papers are briefly summarized; more detailed discussions of the results can be found in the papers.

4.1 Combustion characteristics

4.1.1 Rate of heat release

4.1.1.1 Conventional compression ignition combustion

If alcohol blends are to be used as alternative fuels in non-modified Diesel engines, their rate of heat release profiles should resemble that of fossil Diesel to maintain the engine's controllability. Consistent heat release curves suggest similar peak pressures, pressure rise rates, and engine outputs, which are important for engine durability and the driving experience.

Figure 4-1 shows conventional CI combustion heat release rate curves for Diesel, alcohol/Diesel blends, and fossil-free fuels in the HD and LD engines under reference conditions (an IMEP of 1.02 MPa and engine speed of 1500 for the HD engine, and an IMEP of 0.96 MPa and engine speed of 1280 for the LD engine). A single injection strategy was used in the HD engine, while the multi-injection strategy was applied in the LD engine.

In general, the rate of heat release profiles of the alcohol blends closely match that of fossil Diesel under all tested operating conditions. The variation in SOC between the tested fuels was less than 0.5 CAD at all load points except when using DTBP fuels in the LD engine, in which case the variation was around 1 CAD. ***Figure 4-1 c***, shows results obtained in the LD engine using a pilot injection and a lower boost pressure and compression ratio than were used for the single injection in the HD engine. Because of this, the temperature at SOI in the LD engine was lower than in the HD engine and the ID in the LD engine tests was longer, which could increase uncertainty. Additionally, the DTBP-containing blends appeared to yield more unstable ignition delays between fuels than HVO-containing blends.

The locations of the heat release peaks and the peak values for the fossil-free fuels matched those for fossil Diesel. However, in the HD engine tests, during the mixing-controlled combustion phase after the heat release peaked, fossil Diesel exhibited slightly higher heat release rates than fossil-free fuels. This could be attributed to oxygen content and lower

equivalence ratio of alcohol blends, which may accelerate the combustion process. Moreover, because Diesel has a greater heating value than the blends, its overall rate of heat release curve should be slightly higher given a fixed injection duration.

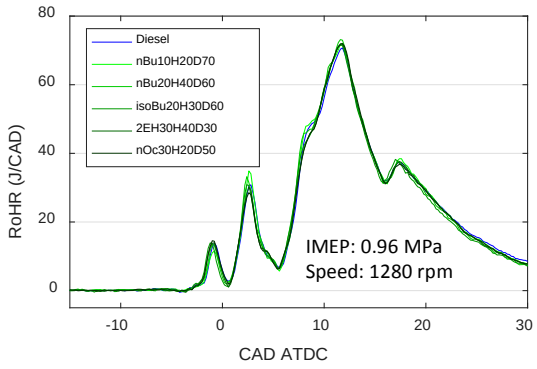

a) Alcohol, Diesel and HVO blends in the LD engine

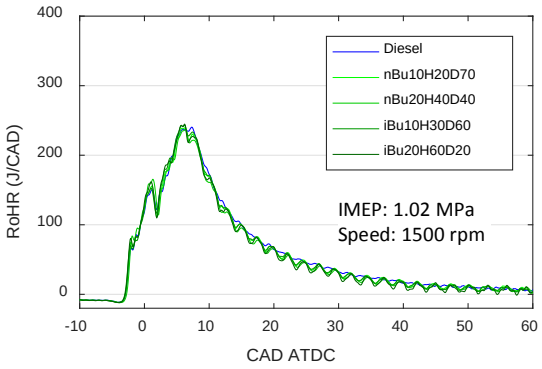

b) Alcohol, Diesel and HVO blends in the HD engine

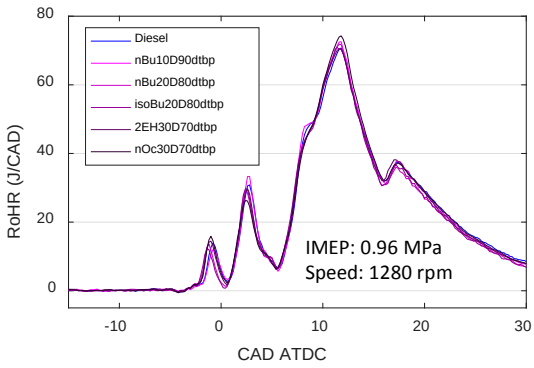

c) Alcohol and Diesel blends with DTBP in the LD engine

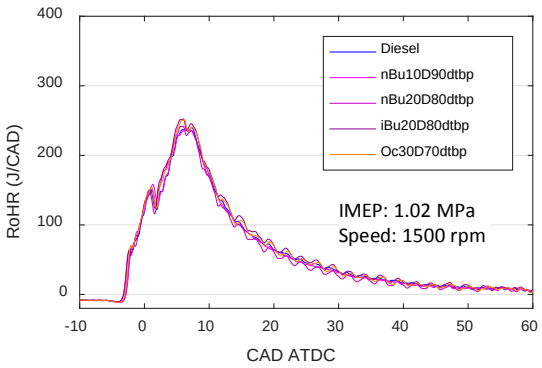

d) Alcohol and Diesel blends with DTBP in the HD engine

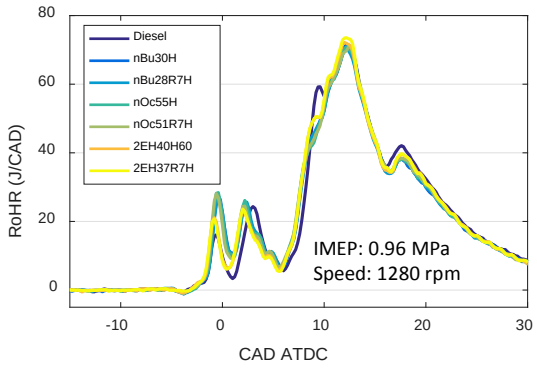

e) Fossil-free blends in the LD engine

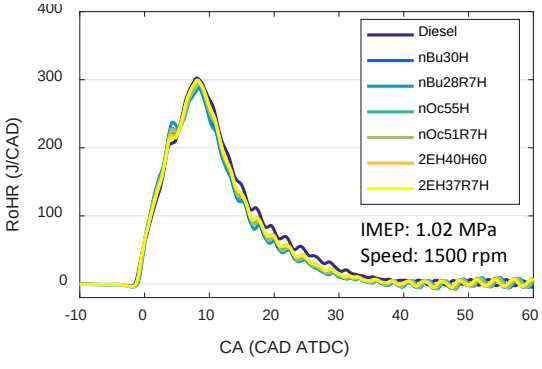

f) Fossil-free blends in the HD engine

Figure 4-1 Conventional CI combustion rate of heat release curves for Diesel and alcohol blends in the HD and LD engines under reference condition. (Paper I and II)

From a combustion point of view, the similar heat release profiles of the alcohol blends and fossil Diesel demonstrate that it is possible to use renewable fuels in unmodified Diesel engines provided that their composition is chosen to match the CN of fossil Diesel.

4.1.1.2 Comparison of wave piston and standard omega piston

Figure 4-2 shows heat release curves for Diesel and the nBu30H blend at the B50 and B75 operating points in the HD engine using two different piston designs: a conventional omega piston and a wave piston. Both fuels yield similar heat release profiles with both piston designs. However, small differences were observed in the mixing-controlled combustion process.

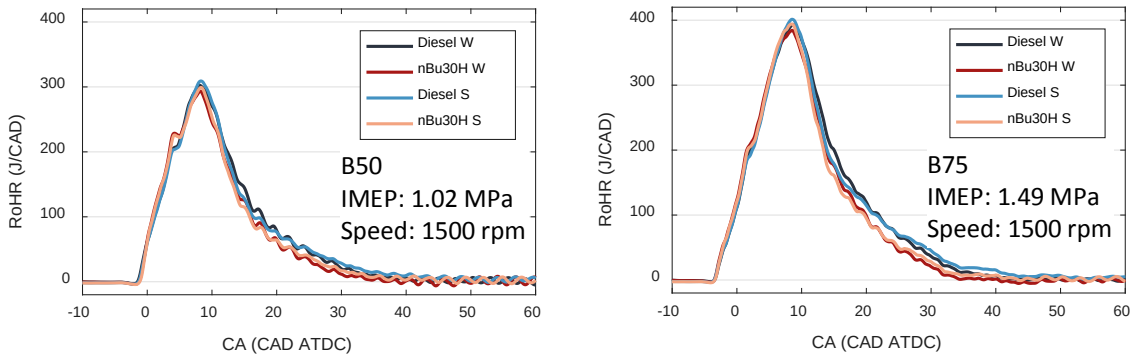

Figure 4-2 Conventional CI combustion rate of heat release curves of Diesel and nBu30H using wave piston and standard omega piston in the HD engine at the B50 and B75.

Figure 4-3 shows how the wave and standard piston designs affected the combustion duration (the length of time between SOC and CA90) for Diesel and nBu30H at the A25, B50, C75, and B75 operating conditions. The black lines in the coloured bars indicate the location of CA50. Replacing the standard piston with the wave design had no effect on SOC for any tested fuel. However, the combustion duration when using the wave piston was clearly shorter than that for the standard piston. The two piston designs yielded similar CA50 values, but the length of time between CA50 and CA90 was shorter for the wave piston than the standard piston. This means that the structure of the wave piston, see ***Figure 3-2***, improves fuel-air mixing and diffusion combustion after the fuel jet hits the 'wave trough' for both Diesel fuel and nBu30H. It may thus be possible to increase an engine's thermal efficiency by replacing conventional pistons with wave piston to accelerate diffusion combustion.

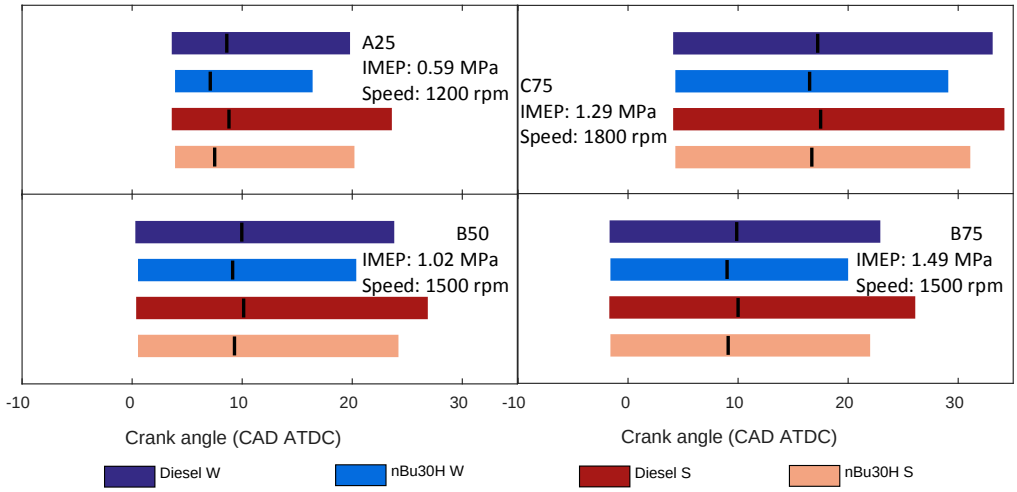

Figure 4-3 Conventinal CI combustion durations (defined as the period between SOC and CA90) achieved using standard and wave piston designs for Diesel and nBu30H at the A25, B50, C75, and B75 operating points.

4.1.1.3 Comparison of conventional CI combustion and PPC

Figure 4-4 shows rate of heat release curves for various low CN fuels at 4 bar IMEP. All fuels generated low temperature reaction in which premixed combustion began after the end of injection, indicating that PPC was achieved.

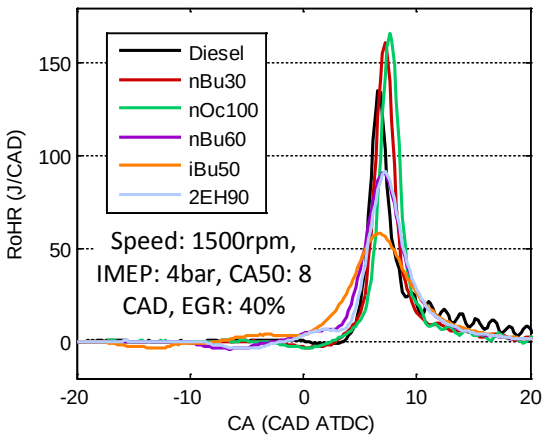

Figure 4-4 Rate of heat release curves for the tested low CN fuels at 4 bar IMEP (Paper III)

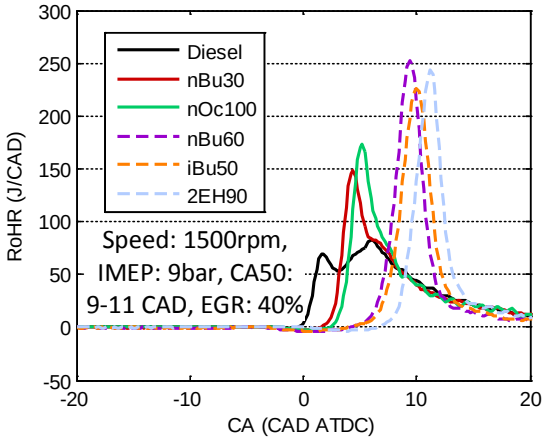

Figure 4-5 Rate of heat release curves for the tested low CN fuels at 9 bar IMEP (Paper III)

Figure 4-5 shows the rate of heat release curves of various fuels at 9 bar IMEP. Three distinct groups of curves can be seen, corresponding to three CN groups. Diesel fuel, which had the highest CN, yielded a typical conventional CI combustion heat release profile with premixed

and diffusion combustion phases. The intermediate CN fuels (CN = 36) nBu30 and nOc100 yielded more premixed combustion before 6 CAD ATDC, at which point there was a step in the curve corresponding to a slowdown in the heat release. The EOI for these fuels occurred almost immediately before SOC, which can be regarded as a critical distinction between conventional CI combustion and PPC. The low CN fuels (CN = 26) nBu60, iBu50, and 2EH90 yielded the highest peak heat release rates and were primarily burned in the premixed combustion phase. Their heat release curves reveal a clear ignition dwell between EOI and SOC, indicating that they have more time to mix with air than the other tested fuels. It was impossible to maintain a CA50 of 8 CAD ATDC when using the low CN fuels without exceeding the maximum tolerable pressure rise rate, so the CA50 was set to the earliest timing consistent with the engine's pressure rise rate limit.

4.1.2 Thermal efficiency

4.1.2.1 Conventional compression ignition combustion

Due to the similar heat release profiles from various fuels with the same CN, the thermal efficiency from them was expected similar during the conventional CI combustion.

Figure 4-6 shows the conventional CI combustion indicated thermal efficiencies of alcohol/Diesel blends with HVO, alcohol/Diesel blends with DTBP, and fossil-free fuels in the HD and LD engines. Fossil Diesel was tested as a reference fuel under all operating conditions.

The operating conditions were found to significantly affect the ITE, but under any given set of operating conditions, all the tested fuels yielded similar ITEs. At the A25 operating point in the HD engine and operating condition 1 in the LD engine, there were no consistent differences between Diesel fuel and the alcohol blends with respect to ITE. However, under the other operating conditions, the blends yielded slightly higher ITEs than Diesel fuel. Under the reference operating conditions (point 2 for the LD engine and B50 for the HD engine), there were no statistically significant differences in ITE between the fuel types. However, on average, the ITEs for the HVO blends, the DTBP blends, and the fossil-free fuel in the LD engine were 1.30 %, 1.74 %, and 0.88 % higher than that for Diesel. The corresponding values for the HD engine were 1.54 %, 1.41 %, and 0.58 %.

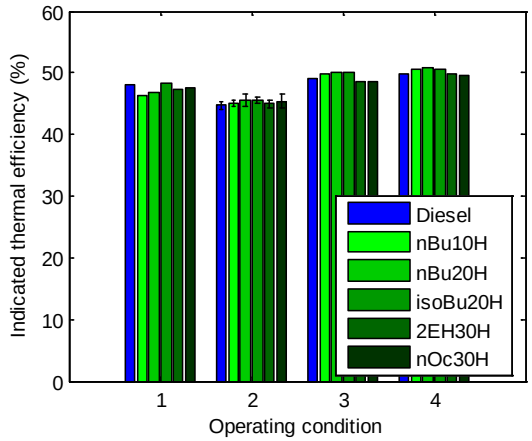

a) Alcohol, Diesel and HVO blends in the LD engine

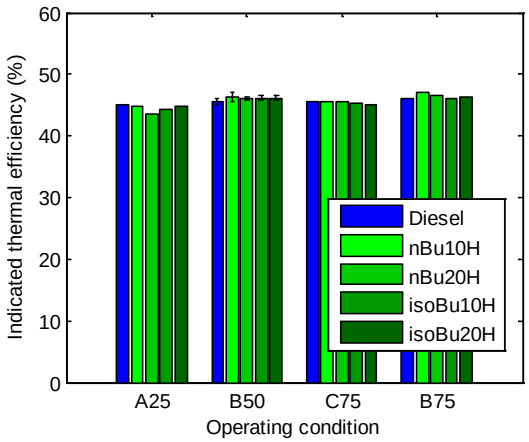

b) Alcohol, Diesel and HVO blends in the HD engine

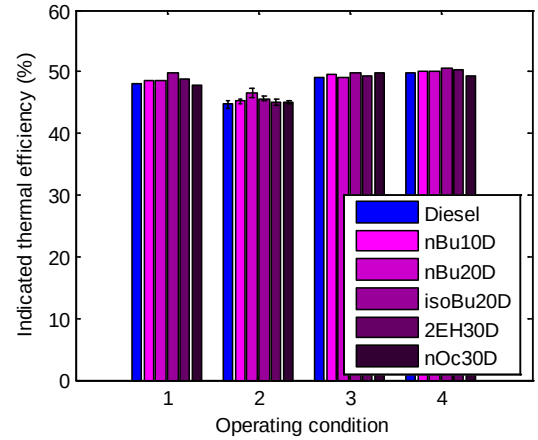

c) Alcohol and Diesel blends with DTBP in the LD engine

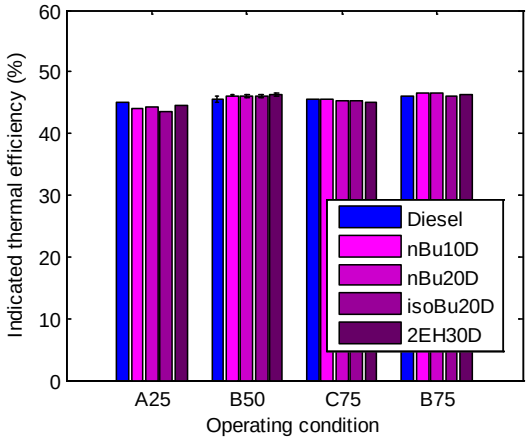

d) Alcohol and Diesel blends with DTBP in the HD engine

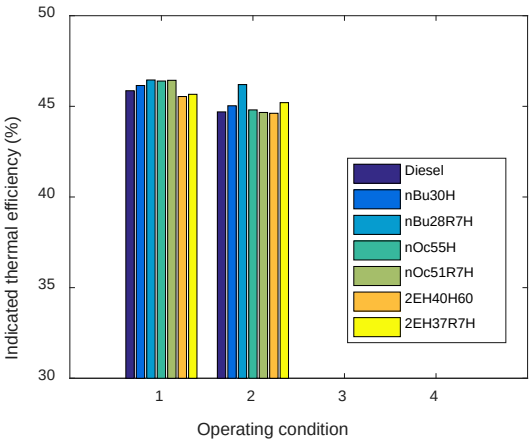

e) Fossil-free blends in the LD engine

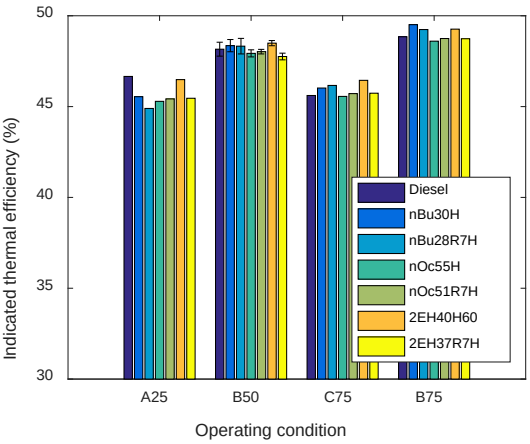

f) Fossil-free blends in the HD engine

Figure 4-6 Conventional CI combustion indicated thermal efficiencies for the tested fuels under various operating conditions. (Paper I and II)

As shown in ***Figure 4-1***, the blends generated slightly faster combustion and shorter combustion durations than Diesel fuel, resulting in slightly higher ITEs. Generally, the larger the energy release close to TDC, the higher the thermal efficiency. [90] In addition, alcohol/Diesel blends promoted complete combustion, which increases thermal efficiency. Finally, because alcohols have lower energy densities and higher latent heats of vaporization than Diesel, they reduce the overall temperature in the cylinder, and so reduce heat transfer losses.

4.1.2.2 Comparison of wave piston and standard omega piston

Figure 4-7 shows the indicated thermal efficiencies of the HD engine when equipped with the wave piston or a standard piston under factory calibration settings and optimized conditions with fixed CA50 of 8 CAD ATDC. Using the production engine settings with Diesel fuel, the wave piston yielded a higher thermal efficiency than the standard piston at the A25, B50, and B75 operating point, but the opposite was seen at the C75 load point. The wave piston tended to reduce the combustion duration (see ***Figure 4-3***), which was the main reason that it yielded higher thermal efficiencies under most conditions. At B50, wave piston produced statistically significant higher the thermal efficiency (0.97 %) than the standard piston. At the C75 operating point, the CA50 was relatively late, so advancing the combustion timing would improve thermal efficiency and increase the effect of the wave piston.

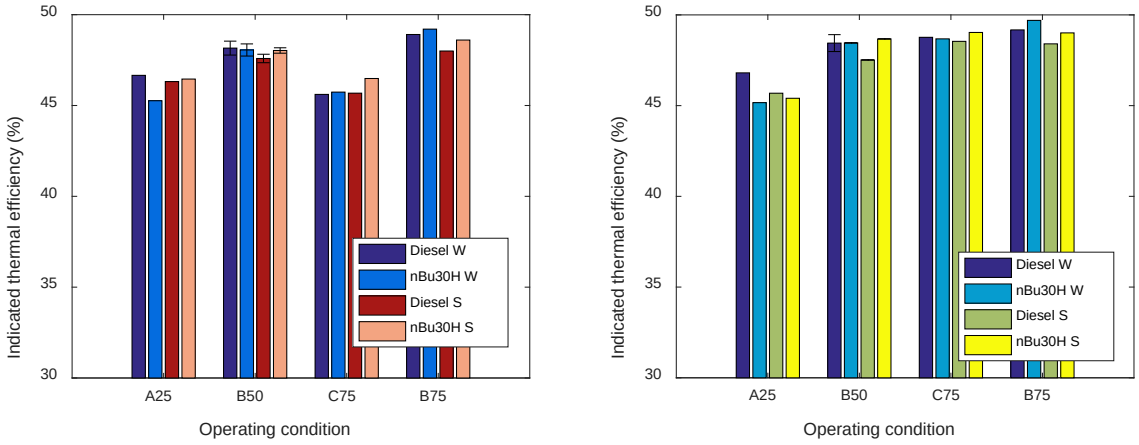

a) Factory calibration settings b) CA50 = 8 CAD ATDC

Figure 4-7 Conventional CI combustion indicated thermal efficiencies when using Diesel and nBu30H in the HD engine with the wave piston and the standard piston at a) factory calibration settings and b) with a fixed CA50 of 8 CAD ATDC.

The thermal efficiencies achieved when CA50 was fixed were higher than those achieved at factory settings, especially for the C75 operating point, because of the advanced combustion. The advanced injection timing at the C75 point enhanced the wave piston's effect because the piston head was closer to the top dead centre. Therefore, the thermal efficiency achieved with the wave piston exceeded that for the standard piston when using Diesel fuel.

When using nBu30H, there were no consistent differences between the ITEs achieved with the two pistons with two types of settings, suggesting that the wave piston's tendency to reduce the combustion duration may not greatly affect the thermal efficiency of combustion with oxygenated fuels. The thermal efficiency achieved using the wave piston was statistically significantly greater than that achieved with the standard piston in experiments with Diesel fuel but not when using the nBu30H blend.

4.1.2.3 Partially premixed combustion

Figure 4-8 shows the indicated thermal efficiency achieved during partially premixed combustion of nBu30 and nBu60 under the reference operating conditions (an engine speed of 1280 rpm and an IMEP of 0.96 MPa) in the LD engine. The indicated thermal efficiencies of both fuels increase with the EGR and lambda in all cases. In addition, for nBu60, the influence of EGR on thermal efficiency appears to become more pronounced above a certain lambda threshold.

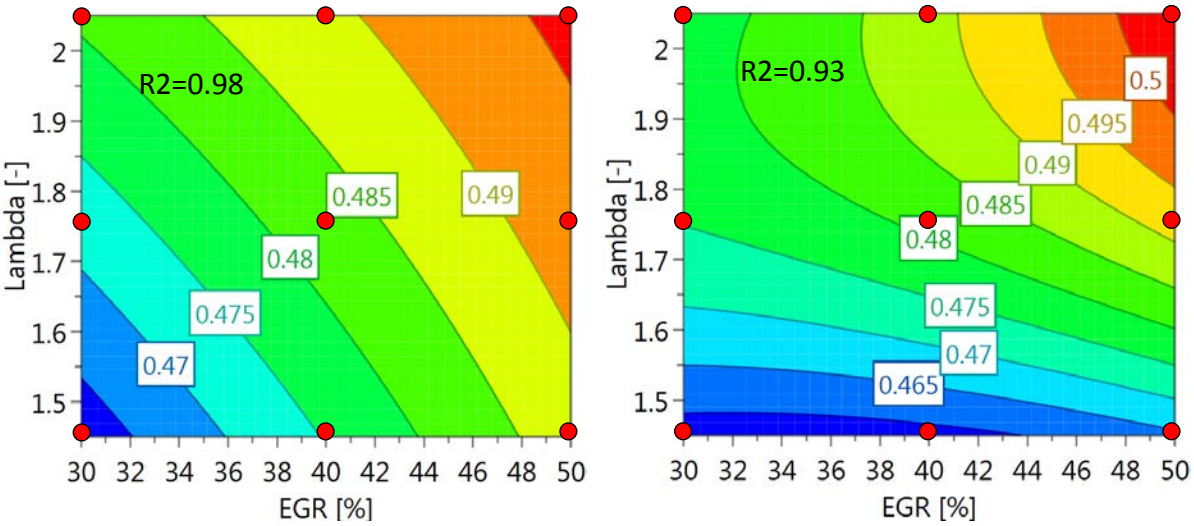

a) nBu30 b) nBu60

Figure 4-8 Indicated thermal efficiency of partially premixed combustion with a) nBu30 and b) nBu60 at an engine speed of 1280 rpm and an IMEP of 0.96 MPa in the LD engine. (Paper III)

The thermal efficiency for conventional combustion at the reference point with Diesel fuel was 44.66 %. The use of low CN fuels improved the indicated thermal efficiency when lambda and the EGR were relatively high. This could be attributed to the fast combustion of the alcohol/Diesel blends. However, the use of low CN fuels and high EGR led to more incomplete combustion, which reduces the thermal efficiency.

4.2 Emissions

4.2.1 Soot emissions

Figure 4-9 shows the indicated specific soot emissions as functions of the fuel's oxygen mass fraction at various operating points of the LD and HD engines. The soot emissions clearly decreased as the fuel's oxygen content increased in both engines.

Several explanations for the lower soot emissions achieved using alcohol blends in Diesel engines have been proposed. The presence of oxygen atoms in the fuel promotes soot oxidation and the consumption of soot precursors by producing hydroxyl radicals, especially in fuel-rich regions. [97,91] In addition, the greater the fuel's oxygen molar fraction, the lower its content of carbon-carbon single and double bonds, and thus the lower the rate of soot formation [92].

The tested alcohol blends had lower stoichiometric A/F ratios than Diesel fuel (see ***Table 2-1***), resulting in lower overall equivalence ratios. Low equivalence ratios thus appear to suppress soot formation.

Short-chain alcohols (butanol, ethanol, and so on) have higher vapour pressures and lower boiling points and viscosities than Diesel fuel, facilitating the breakup and evaporation of their blends. This in turn improves fuel-air mixing and suppresses soot formation. [93] However, this does not explain the low soot emissions achieved with octanol blends because the octanol isomers are more viscous and have similar boiling points to Diesel fuel (see ***Table 2-1***).

Alcohols' low CN values result in longer ignition delays and thus more uniform fuel-air mixtures. [94] However, all the fuels tested in this work had similar CN values and ID and so generated similar premixed combustion fractions. Despite this, the blends generated significantly lower soot emissions than fossil Diesel. The flame lift-off length of the fuel is recognized as a key factor affecting soot formation and oxidation [82,95]. However, all the fuels studied in this work had similar ignition delay times to Diesel fuel, implying that they should also have similar flame lift-off lengths (see ***Figure 4-12***). Given the fuels' similar CN and ignition delay times, their lift-off lengths are unlikely to have influenced the variation in their soot emissions as much as other conditions.

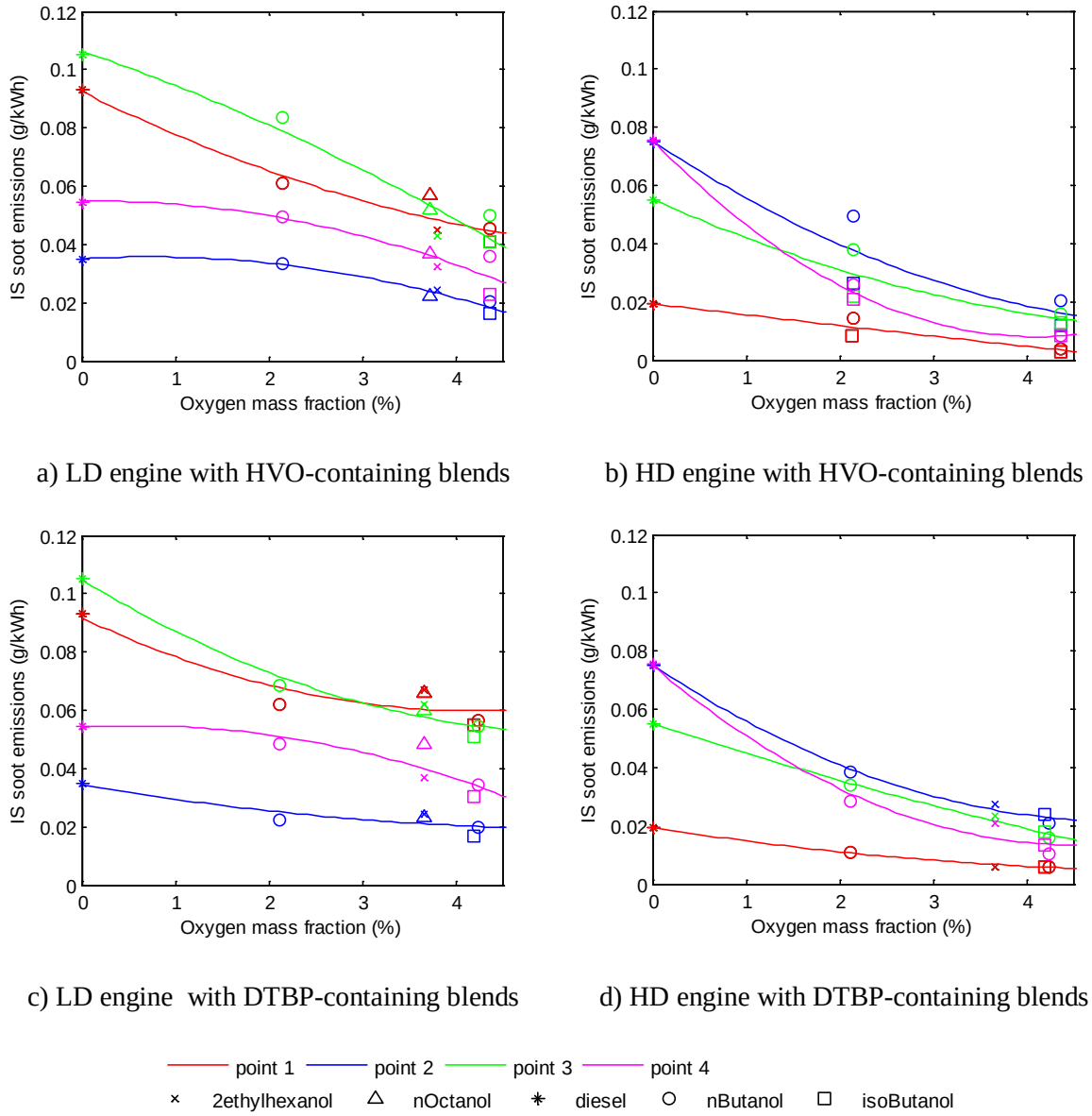

Figure 4-9 Conventional CI combustion indicated soot emissions plotted against the fuel's oxygen mass fraction at four operating points for (a) LD and (b) HD engines with HVO-containing blends, and (c) LD and (d) HD engines with DTBP-containing blends. (Paper I and II)

In addition, the reductions in soot emissions achieved with the alcohol blends were more pronounced in the HD engine than in the LD engine. A multi-injection strategy was used in the LD engine tests, which enhances fuel-air mixing and thus reduces the fuel fuel-rich region. Therefore, the soot-reducing effects of the alcohols were weakened in the LD engine. Yao et al. [49] have also suggested that the soot reduction effect of post injection decreases with increasing *n*-butanol fraction in Diesel, because presence of *n*-butanol may cause poor mixing

and oxidation by reducing the blend spray's momentum (due to the alcohol's lower density) and energy content (due to the alcohol's lower heating value).

HVO-containing blends generated less soot than DTBP-containing blends because they contained less fossil Diesel and HVO is free of aromatic compounds.

Figure 4-10 shows the indicated soot emissions in the HD engine equipped with a wave piston or a standard piston under a) factory calibration settings and b) optimized condition with fixed CA50 of 8 CAD ATDC. At the production engine settings, Diesel fuel produced lower or similar soot emissions when using wave piston than that of using standard piston, except operating condition C75. More homogeneous fuel air mixing reduces the equivalence ration and suppresses the soot formation. Under C75, injection timing and CA50 was relatively late, which weakened the effect of promoting fuel air mixing from the wave piston. When advancing the injection timing in ***Figure 4-10 b***, Diesel fuel produced similar soot emissions for using the wave piston and standard piston at C75.

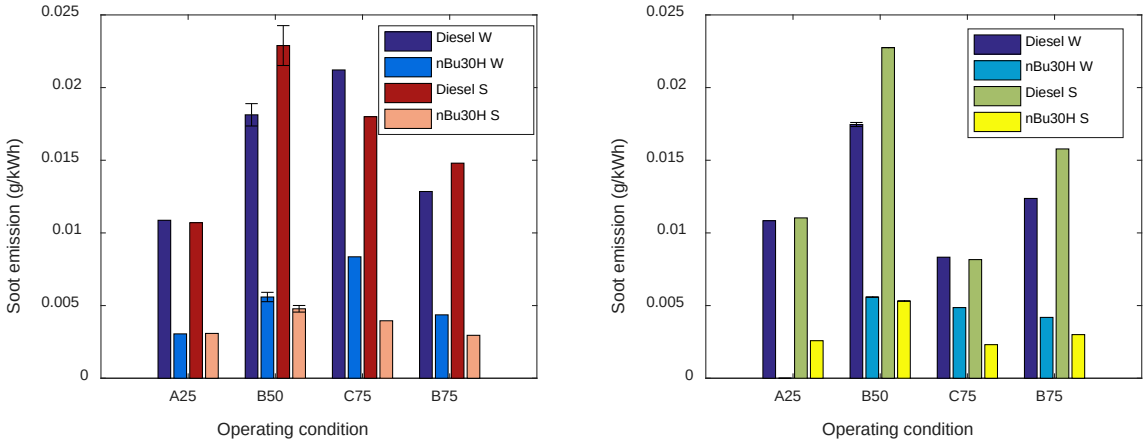

a) Production engine settings

b) Production engine settings but fixed CA50 = 8 CAD ATDC

Figure 4-10 Conventional CI combustion comparison of soot emissions generated with a wave piston and a standard piston in an HD engine under (a) production engine settings (b) CA50 = 8 CAD.

The soot reducing effect of the wave piston was less pronounced for nBu30H, in keeping with the thermal efficiency measurements shown in ***Figure 4-7***. When using nBu30H, the fuel-air mixing process is boosted by the high volatility of *n*-butanol compared to Diesel. Therefore, it would be difficult to improve the mixing further. Moreover, the liquid penetrations of Diesel and nBu30H were different, so the tuned injection strategy and optimized injector nozzle may ameliorate the effect of fuel air mixing using the wave piston for nBu30H.

4.2.2 *Particulate matter in the constant volume combustion chamber*

Figure 4-11 shows soot emissions during steady-state fuel combustion in the constant volume combustion chamber as a function of the flame lift-off length, ignition delay time, oxygen mass fraction in the fuels, and stoichiometric A/F ratio. Combustion was performed at an ambient temperature and air density of 823 K and 26 kg/m^3, and the injection pressure was 120 or 180 MPa. The soot emissions in the figures were calculated from the soot volume fraction according to ***Equation 3.33***.

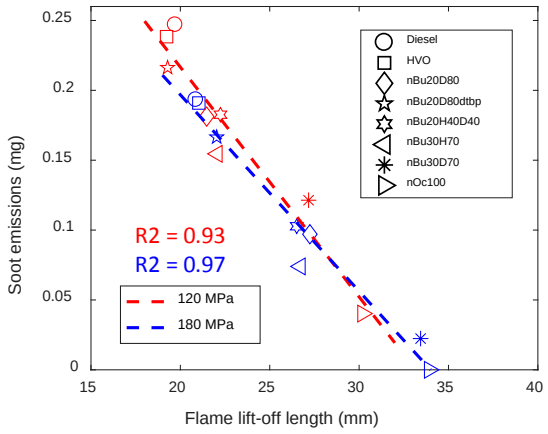

a) Soot emissions versus flame lift-off length

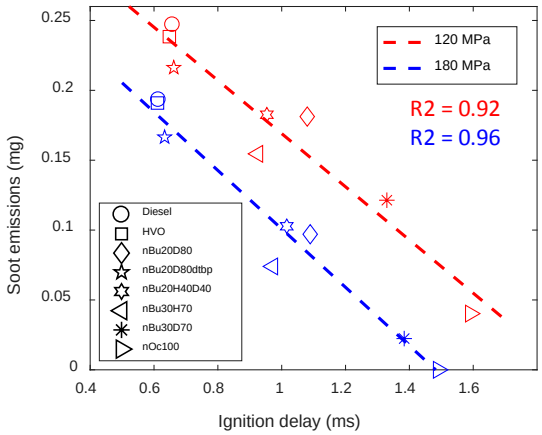

b) Soot emissions versus ignition delay

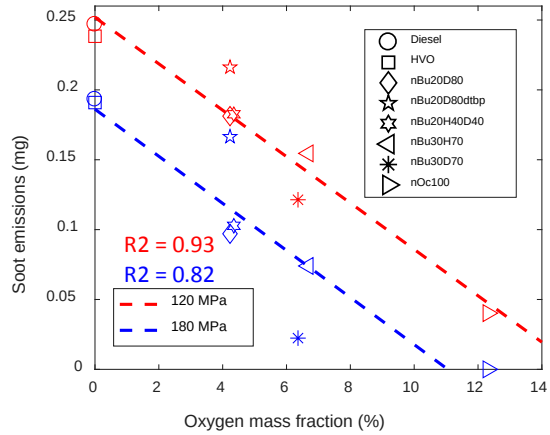

c) Soot emissions versus oxygen mass fraction in the fuels

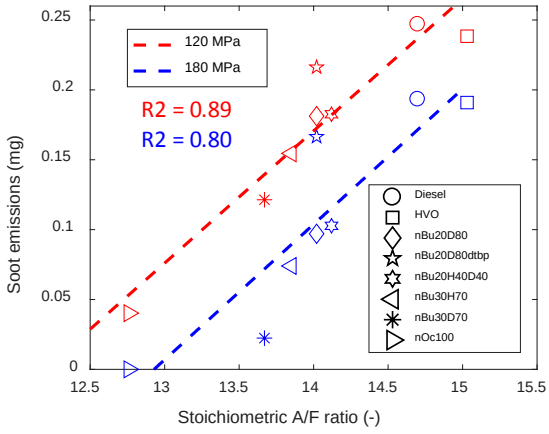

d) Soot emissions versus stoichiometric A/F ratio

Figure 4-11 Soot emissions during steady state combustion at an injection pressure of 120 and 180 MPa plotted against the a) flame lift-off length, b) ignition delay time, c) oxygen mass fraction in the fuel, and d) stoichiometric A/F ratio.

Figure 4-11 a shows that there was a good linear correlation between soot emissions and flame LOL, indicating that soot emissions declined as the flame LOL increased at both studied injection pressures. Longer LOLs result in more extensive air entrainment and reduce the equivalence ratio at the LOL, thus reducing soot formation and increasing soot oxidation. Varying the injection pressure had little apparent influence on the relationship between LOL and soot emissions because higher injection pressures increase the fuel jet's velocity and thus increase the LOL. [96] No soot was detected when using nOc100 at an injection pressure of 180 MPa.

Figure 4-11 b shows that the ignition delay time is strongly correlated with soot emissions, especially at an injection pressure of 180 MPa. Longer ignition delays reduce soot emissions because they enable more extensive fuel-air premixing. The ignition delay is closely related to the flame LOL, as discussed later. Increasing the injection pressure reduced soot emissions further.

Figure 4-11 c shows that as the fuel's oxygen mass fraction increased, soot emissions fell. The oxygen atoms in the alcohol components of the blends reduce the local carbon oxygen ratio and have been suggested to suppress soot formation by reducing the concentration of soot precursors [97]. Higher injection pressure improve fuel-air mixing and thus further reduce soot emissions.

Figure 4-11 d shows that soot emissions increase with the stoichiometric A/F ratio, although the correlation coefficient was slightly smaller than for the other three variables. Lower stoichiometric ratios imply lower equivalence ratios in the downstream region of the fuel jet, resulting in lower soot emissions.

The flame lift-off length, ignition delay, oxygen mass fraction, and stoichiometric ratio influence soot emissions via various interdependent mechanisms. The flame lift-off length can be predicted using the following expression [96]:

$$LOL \propto \frac{\mu_0 Z_{st} D}{s_L^2(Z_{st})} \qquad (4.1)$$

where μ_0 is the fuel jet velocity at the nozzle exit, Z_{st} is the stoichiometric fuel fraction (defined as the fuel mass divided by the mixture mass), D is the thermal diffusivity, and S_L is the laminar flame speed for a stoichiometric fuel fraction. The ignition delay can be estimated as [98]:

$$\tau_{ig} = Aexp(E/RT_a){\rho_a}^n {Z_{st}}^m \qquad (4.2)$$

where A is a pre-exponential constant, E is the global activation energy, R is the universal gas constant, ρ_a is ambient air density, and n and m are empirical constants that may vary from fuel to fuel.

The results obtained also suggested a relationship between the ignition delay and the flame lift-off length. ***Figure 4-12*** shows the flame lift-off length under quasi-steady-state conditions as a function of the ignition delay for the tested fuels at an ambient temperature and air density of 823 K and 26 kg/m^3. The dashed lines show linear fits of the LOL at each injection pressure, and the error bars represent the standard deviations of the flame LOL and ignition delay over 30 injection events.

The LOL increases with the ignition delay at both injection pressures, suggesting that fuels with longer ignition delays also have a longer flame LOLs under the studied operating conditions. Kook et al. [99] reported similar results for non-oxygenated Diesel-like fuels, and Jakob et al. [100] observed a comparable relationship between LOL and ignition delay in an optical light duty engine.

The relationship between CN and ignition delay time in the constant volume combustion chamber differed from that seen in the CFR engine. ***Figure 4-13*** shows the average ignition delay times of the tested fuels for injection pressures of 120 MPa and 180 MPa at an ambient temperature and gas density of 823 K and 26 kg/m^3.

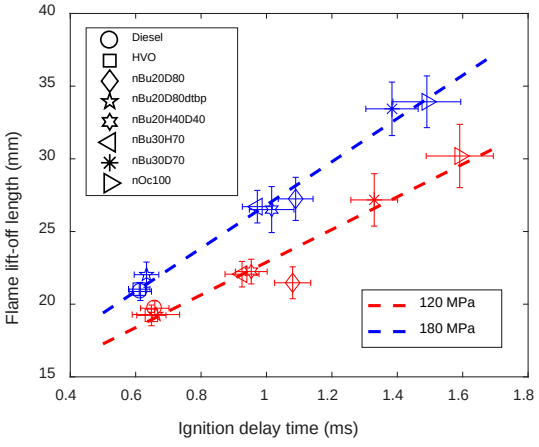

Figure 4-12 Flame lift-off length as a function of the ignition delay time (Paper IV)

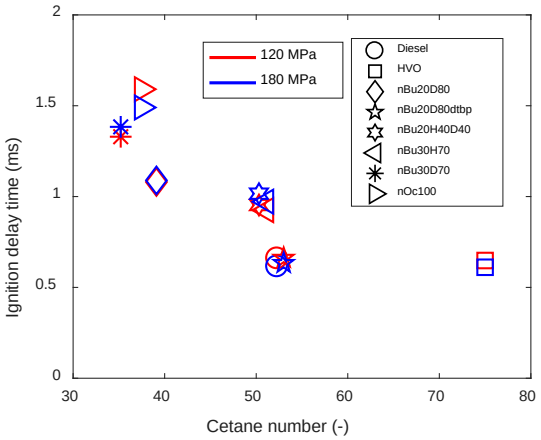

Figure 4-13 Ignition delay as a function of CN in the constant volume chamber

CN measurements conducted in CFR engines suggest that the ignition delay time generally increases with decreasing CN. However, despite having different CNs, neat Diesel and HVO

generated very similar ignition delay times at both injection pressures. Moreover, two HVO-containing blends, nBu20H40D40 and nBu30H70, had longer ignition delays than Diesel and nBu20D80dtbp, despite all four tested fuels have approximately the same CN of 52. These results are inconsistent with the earlier measurements (see ***Figure 4-1***) of ignition quality under the same load conditions in a Diesel engine. It seems that the auto-ignition ability of long chain alkanes under the tested low temperature and low pressure conditions is unremarkable, but the inclusion of DTBP causes early auto-ignition as observed under engine conditions. Increasing the injection pressure from 120 MPa to 180 MPa had little effect on the ignition delay.

4.2.3 Particulate matter size distribution

Figure 4-14 shows the conventional CI combustion particulate matter size distributions for the LD and HD engines under the reference operating conditions using alcohol blends and Diesel in. In the LD engine, the distribution curves were all unimodal, the single peaks located between 75 and 105 nm for all tested fuels. Diesel fuel generated higher particulate number concentrations than other fuels, especially for larger particles, which is consistent with the higher soot emissions generated with Diesel fuel. Replacing Diesel with the alcohol blends had no clear effect on the concentration of nucleation mode particles with diameters below 50 nm.

In the HD engine, most fuels generated bimodal particulate matter size distributions with a distinct nucleation mode peak between 6 and 10 nm and a separate accumulation mode peak between 70 and 90 nm. Unlike in the LD engine, Diesel fuel yielded higher concentrations of accumulation mode particles while fossil-free alcohol blends generated higher concentrations of nucleation mode particles in the HD engine.

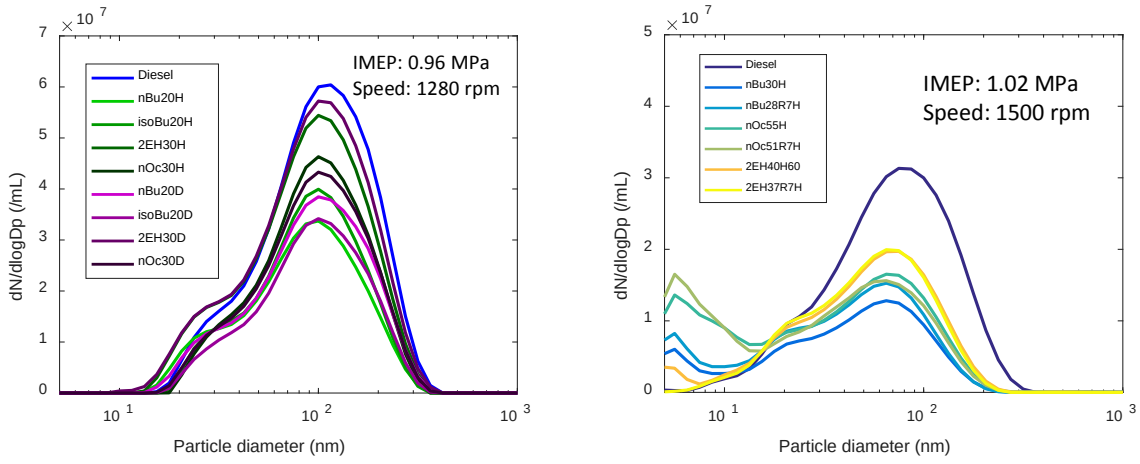

a) LD engine data b) HD engine data

Figure 4-14 Particulate matter size distributions in the (a) LD and (b) HD engines. (Paper II)

The higher concentration of small particles generated in the HD engine was investigated further. ***Figure 4-15*** shows the particle size distributions for the HD engine using five fuels. Butanol and octanol blends produced fewer accumulation mode particles and thus provided a smaller surface area for coagulation and agglomeration, resulting in higher nucleation mode particles.

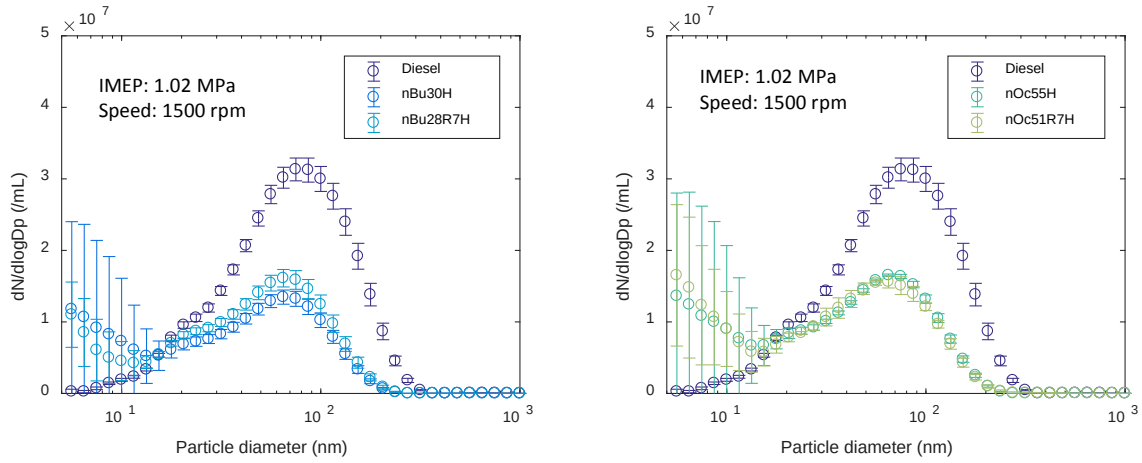

a) Particle size distributions for butanol blends b) Particle size distributions for octanol blends

Figure 4-15 Conventional CI combustion particle size distributions for (a) n-butanol blends and (b) n-octanol blends in the HD engine.

The concentrations of small particles (diameter < 20 nm) generated by burning butanol and octanol blends varied widely, but burning Diesel fuel produced consistent small variations in particle concentration over the whole size range. The temperature of the exhaust plenum and exhaust pipes (see ***Figure 3-3***) influenced a lot by previous operating condition at the reference operating condition with a steady engine-out exhaust temperature, explaining the variation in nuclear particle concentration. Hellier reported [101] that the concentration of nucleation mode particles correlated with the boiling points of the fuel molecules, suggesting that condensation of unburned fuel may be important in the formation of these small particles. Variation in the sampling temperature in the exhaust pipe may influence the oxidation, cooling and dilution processes, and thus nucleation mode particle formation. [102] Similar variability in nucleation mode particle concentration was reported by Gontaras [103].

4.2.4 NO_x emissions

There are three widely accepted mechanisms of NO_x formation: thermal NO_x, prompt NO_x, and fuel NO_x. [104] Zeldovich thermal activation is the most significant pathway for NO_x formation via the high-temperature reaction of nitrogen with oxygen during conventional CI combustion in internal combustion engines. High cylinder temperatures and local oxygen concentrations

and long residence times in the peak temperature zone all favour NO_x formation. Prompt NO_x is formed by a relatively fast reaction, which is an important mechanism of NO_x formation in low-temperature combustion processes but much less important than thermal NO_x in high temperature environments. The fuel NO_x mechanism involves nitrogen atoms bound to fuel molecules as amines and was not an important mechanism in the context of this work.

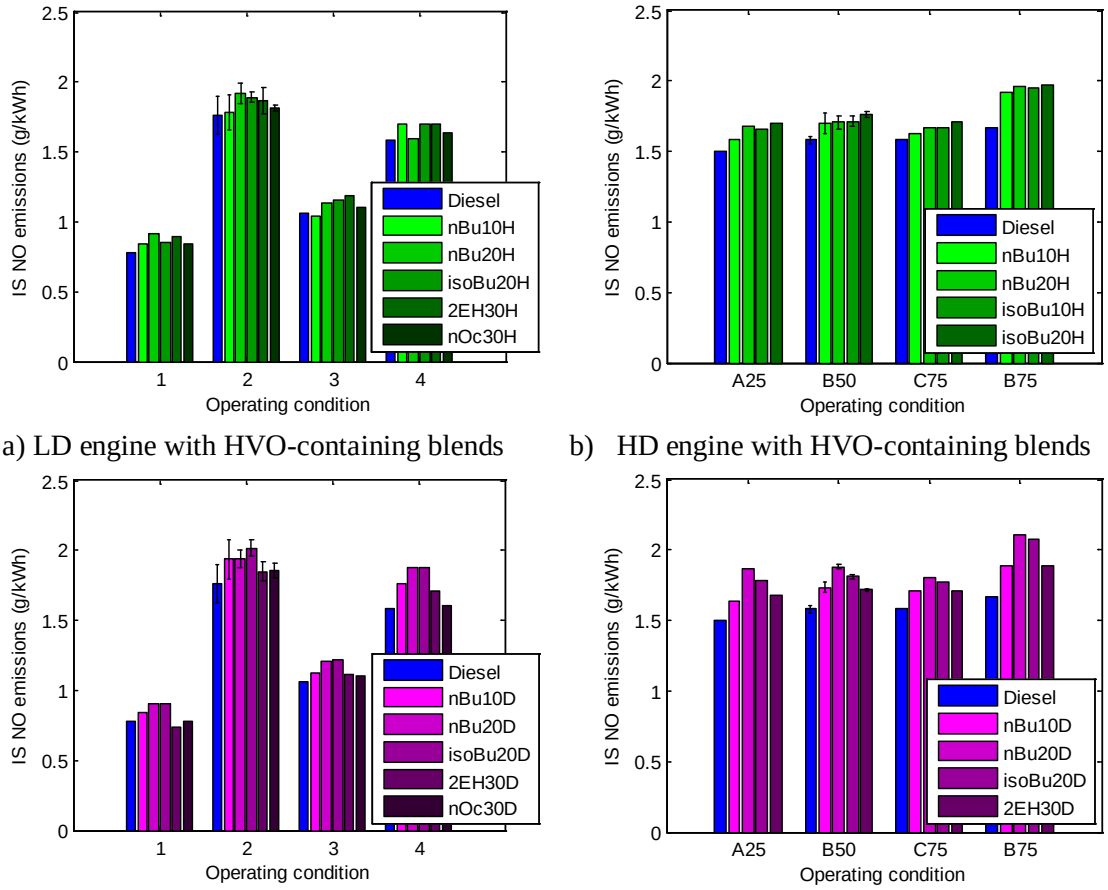

a) LD engine with HVO-containing blends b) HD engine with HVO-containing blends

c) LD engine with DTBP-containing blends d) HD engine with DTBP-containing blends

Figure 4-16 Conventional CI combustion indicated specific NO emissions generated under various conditions with HVO-containing blends in the (a) LD and (b) HD engines, and with DTBP-containing blends in the (c) LD and (d) HD engines. (Paper II)

The main constituent of NO_x emissions is NO, especially at medium and high loads in Diesel engines [90]. Therefore, NO emissions generated when using Diesel fuel and the alcohol blends were measured. ***Figure 4-16*** shows indicated specific NO emissions generated under various operating conditions in the LD and HD engines fuelled with HVO-containing and DTBP-containing blends. For both engines, the alcohol/Diesel blends generated more NO emissions than Diesel fuel. As mentioned before, alcohol blends induce faster combustion than Diesel fuel, which may result in higher peak local temperatures. In addition, the present of oxygen in

the fuel reduces the equivalence ratio. High in-cylinder temperatures and low equivalence ratios promote Zeldovich thermal activation and NO formation.

The NO emissions generated with the HVO- and DTBP-containing blends in the LD and HD engines engine were statistically significantly greater (by 6.8 % and 8.9 %, respectively, for the LD engine and 14.6 % and 10.4 %, respectively, for the HD engine) than those generated with Diesel fuel. It seems that using DTBP as ignition improver may slightly increase the combustion temperature and NO emissions.

Figure 4-17 shows the NO_x emissions generated using the wave and standard pistons at various operating points in the single cylinder HD engine. Diesel fuel and nBu30H produced more NO_x emissions when using wave piston due to its promotion of fuel air mixing and flame propagation, both of which favour higher combustion temperatures.

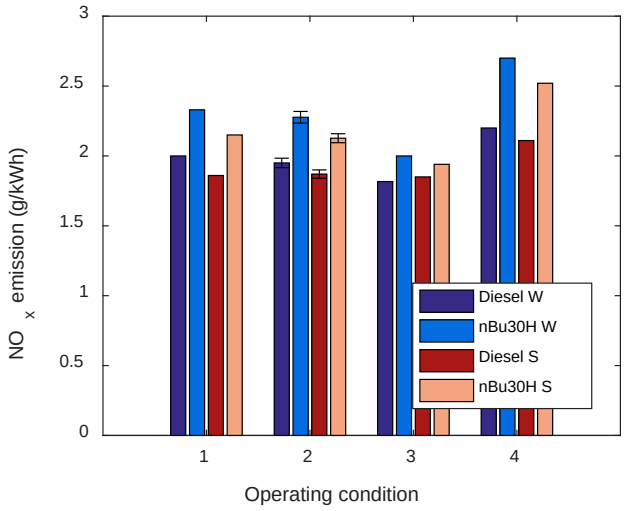

Figure 4-17 Conventional CI combustion NO_x emissions generated using the wave and standard pistons at various operating points in the HD engine.

Figure 4-18 shows the soot-NO trade-off curves for partially premixed combustion as functions of the EGR. For alcohol blends, NO emissions decreased with the EGR increase (from 25 to 55%). Conversely, varying the EGR had little effect on soot emissions, especially for the low CN fuels (nBu60, iBu50, and 2EH90). Despite having similar CNs and combustion processes, nBu30 and nOc100 had clearly different soot-NO trade-off curves. The fuel of nOc100 contains no fossil Diesel, which may be why it produced lower soot emissions than nBu30 (which contains 70 % Diesel). Large molecules (notably, aromatics) in Diesel would facilitate soot formation. Conversely, the oxygen mass fraction of nOc100 is greater than that of Diesel, which

would tend to reduce soot emissions. Both soot and NO emissions could be reduced by combining low CN fuels and optimized EGR with partially premixed combustion.

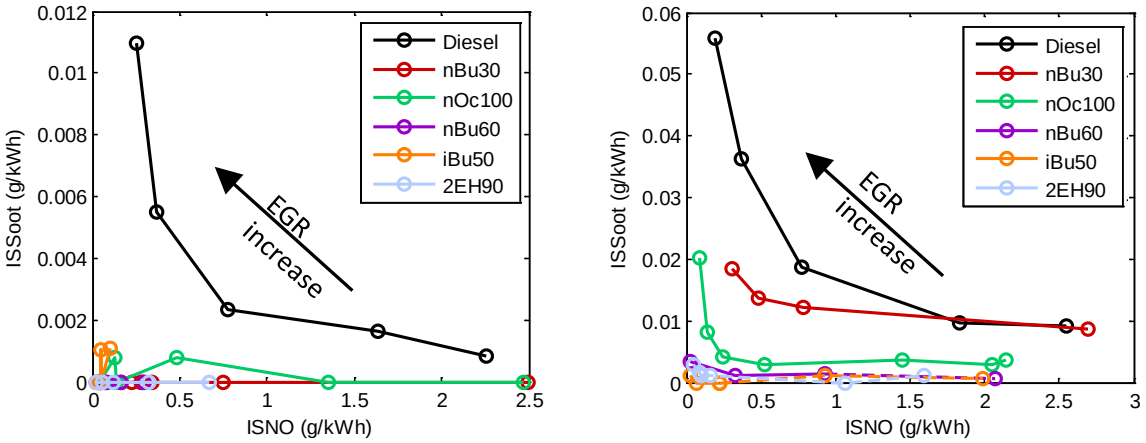

a) IMEP = 4 bar b) IMEP = 9 bar

Figure 4-18 Partially premixed combustion soot-NO trade-off curves as functions of the EGR at a) 4 bar IMEP and b) 9 bar IMEP. In all cases, CA50 = 8 CAD ATDC or the earliest possible value, and lambda = 2.0. (Paper III)

4.2.5 CO emissions

For conventional CI combustion, the effects of the studied fuels on CO emissions in the LD and HD engines were similar, so only results for the HD engine are discussed here.

Figure 4-19 shows the indicated specific CO emissions generated using Diesel and the various alcohol blends at the A25, C75, B50 and B75 operating conditions in the HD engine. The CO emissions mirror the trends seen for soot emissions, declining as the fuel's alcohol content increases. As discussed in the section on soot emissions, lower equivalence ratios promote complete fuel combustion (and thus CO oxidation), [49] so the alcohol blends yielded statistically significantly lower CO emissions than Diesel fuel. Specifically, the CO emissions for nBu10H, nBu20H, iBu10H, and iBu20H at the B50 operating point were 16 %, 29 %, 24 %, and 35 % lower, respectively, than that for Diesel. The corresponding values for the DTBP-containing blends nBu10D, nBu20D, iBu20D, and 2EH30D were 19 %, 32 %, 30 %, and 25 %, respectively.

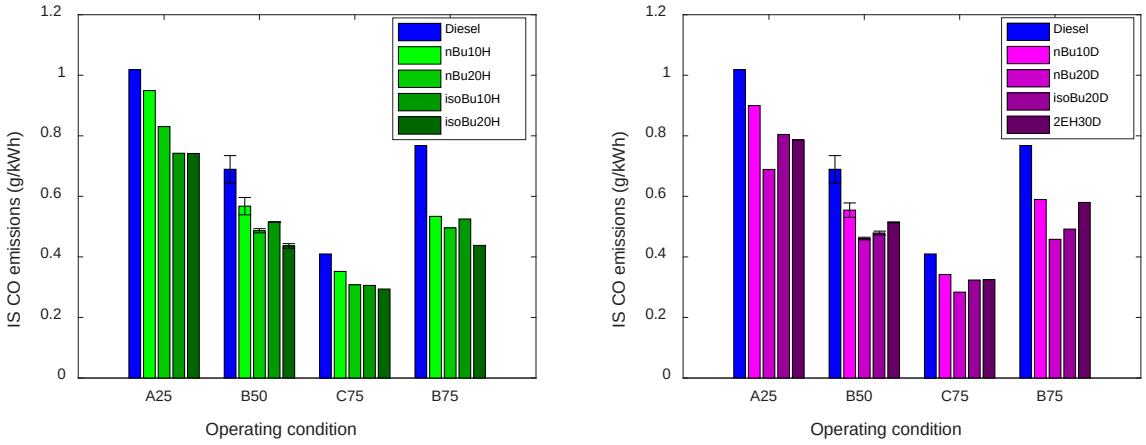

a) HVO-containing blends b) DTBP-containing blends

Figure 4-19 Conventional CI combustion indicated specific CO emissions generated using a) HVO-containing blends and b) DTBP-containing blends at A25, C75, B50 and B75 in the HD engine. (Paper I)

Figure 4-20 shows the CO emissions achieved with fossil-free fuels under various operating conditions in the HD engine in conventional CI combustion. In accordance with the results shown in ***Figure 4-19***, fossil-free blends generated lower CO emissions than Diesel under all conditions except A25. At the B50 operating point, the fossil-free fuels yielded statistically significantly (between 15 % and 21 %) lower CO emissions than fossil Diesel.

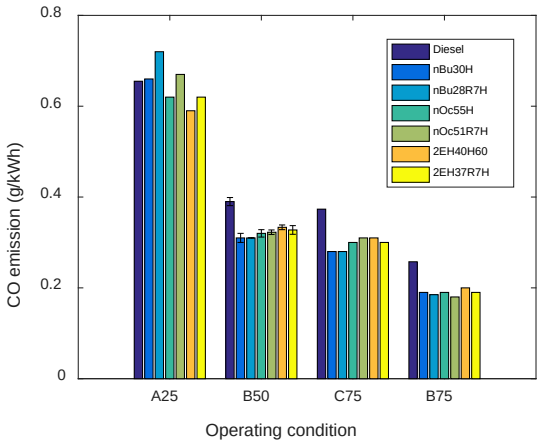

Figure 4-20 CO emissions of fossil-free fuels under various operating conditions.

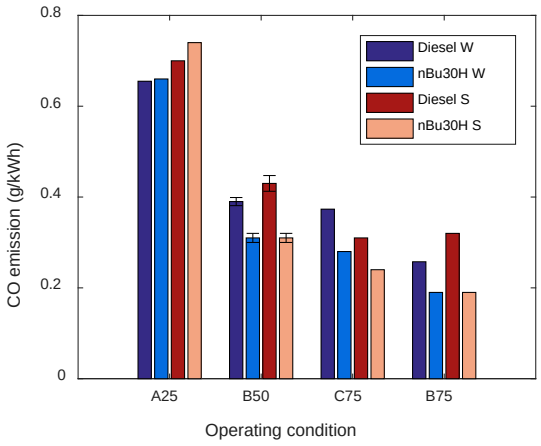

Figure 4-21 Comparison of wave piston and standard piston on CO emissions.

Figure 4-21 compares the CO emissions achieved with the wave and standard pistons. The use of the wave piston reduced the CO emissions at the A25, B50, and B75 points for Diesel. With advanced CA50, a reduction of CO could be measured at C75 by using wave piston.

Figure 4-22 shows the PPC indicated CO emissions of nBu30 and nBu60 at an engine speed of 1280 rpm and IMEP of 0.96 MPa in the LD engine. In general, the CO emissions increase as the EGR increases and lambda decreases for both nBu30 (nBu30D70) and nBu60 (nBu60D40). Increasing the EGR and reducing lambda will reduce the in-cylinder temperature and the oxygen concentration. In-cylinder temperature is the key factor governing the CO emissions under the studied conditions. At temperatures below 1500 K, the conversion of CO into CO_2 will be slow. Reducing the EGR or increasing lambda raise the combustion temperature, facilitating CO oxidation. Low oxygen concentrations also favour incomplete oxidation.

Similar load point was performed in a conventional CI combustion system with fossil Diesel. The specific CO emission is 0.68 g/kWh from the conventional CI combustion. The similar results could be reached for nBu30 when the EGR kept around 40 %, while for nBu60 the boost pressure must be much higher to increase the lambda to achieve the conventional CI combustion CO emission level.

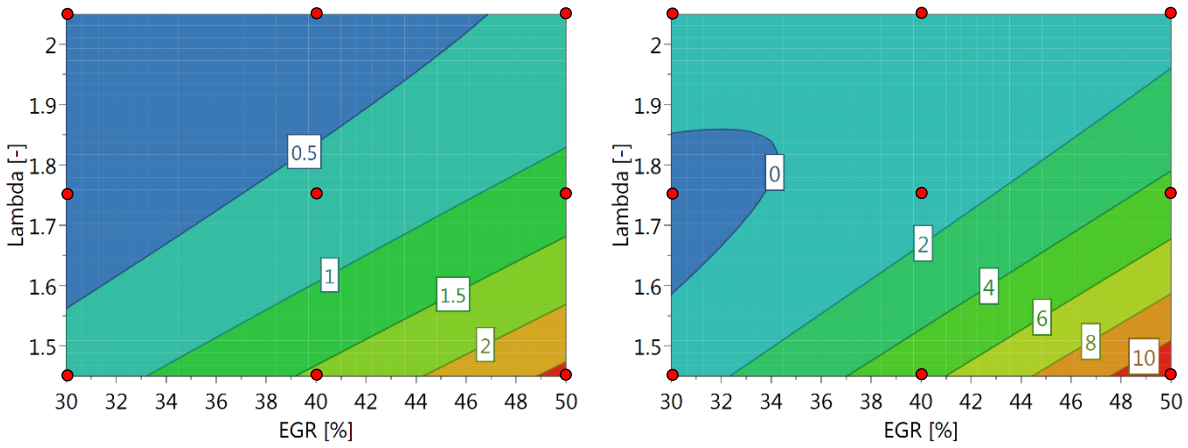

a) nBu30 b) nBu60

Figure 4-22 Partially premixed combustion indicated CO emissions of a) nBu30 and b) nBu60 at the engine speed of 1280 rpm and IMEP of 0.96 MPa in the LD engine.

4.2.6 HC emissions

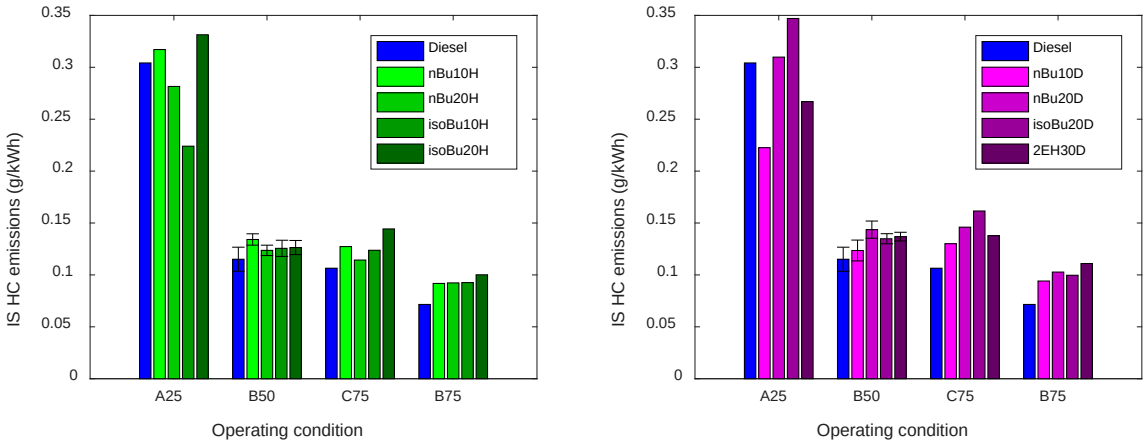

a) HVO-containing blends

b) DTBP-containing blends

Figure 4-23 Conventional CI combustion indicated specific HC emissions generated using a) HVO-containing blends and b) DTBP-containing blends at A25, C75, B50 and B75 in the HD engine. (Paper II)

Figure 4-23 shows the conventional CI combustion indicated specific HC emissions for Diesel and the tested alcohol blends at the A25, C75, B50, and B75 operating conditions in the HD engine. Combustion of the blends produced slightly higher HC emissions than those from fossil Diesel, especially at high load points. At B50, only nBu10H and nBu20D statistically significant increased HC emissions (by 18.2 % and 26.7 % compared to Diesel, respectively). In general, the HC emissions were highly variable, obscuring any potential effect of alcohol-containing fuels.

Even under the A25 conditions (i.e. the conditions yielding the highest HC emissions), the emissions for the alcohol blends were below the Euro 5 limit (0.46 g/kWh). The differences in HC emissions between the different fuels were most pronounced at the lowest load (A25). This may be because the quantity of injected fuel is lowest under the A25 conditions and the EGR is the highest, making for less stable combustion and higher HC emissions.

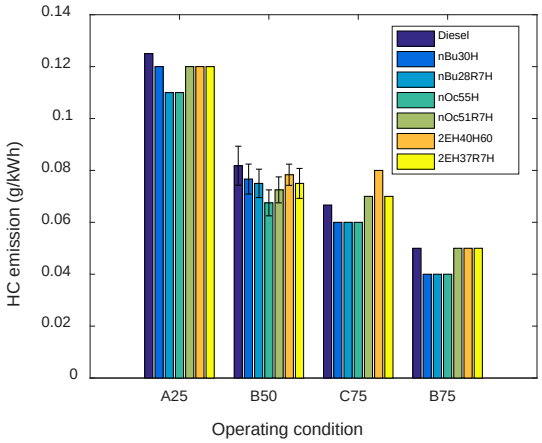

Figure 4-24 HC emissions of fossil-free fuels at various operating conditions in the HD engine.

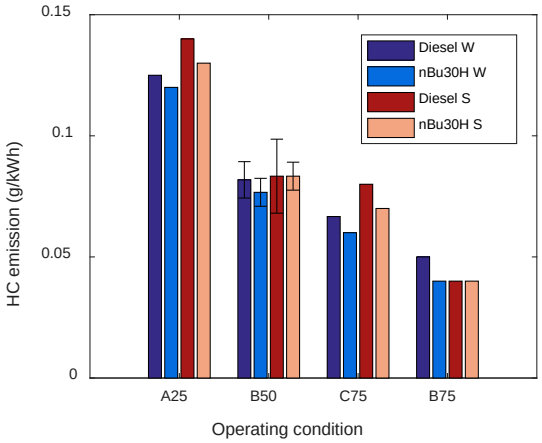

Figure 4-25 The wave and standard pistons' effects on HC emissions.

Figure 4-24 shows the conventional CI combustion HC emissions of fossil-free fuels under various operating conditions in the HD engine. Fossil-free fuels and Diesel appeared similar HC emissions under all tested operating conditions, and the values were all below the EURO 6 HC emission threshold (0.13 g/kWh). These results are lower than those shown in ***Figure 4-23***, due to the use of a bigger engine.

At B50, the differences between Diesel and fossil-free fuels were not statistically significant because of their similarity and relatively high variation (9.18 %). HC emissions declined as the load increased because the higher in-cylinder temperatures at the higher load led to more complete oxidation of unburned HC emissions.

Figure 4-25, shows that the HC emissions achieved using the wave piston did not differ significantly from those achieved with the standard omega piston in the HD engine.

Figure 4-26 shows the PPC indicated HC emissions of nBu30 and nBu60 at an engine speed of 1280 rpm and an IMEP of 0.96 MPa in the LD engine. The HC emissions did not vary greatly over a wide range of EGR and lambda values when using nBu30. For nBu60, the HC emissions increased as the EGR rate increased and lambda decreased, which is consistent with the trend in CO emissions. Increasing the EGR rate and reducing lambda will reduce in-cylinder temperatures and oxygen concentrations, leading to incomplete oxidation. The lower in-cylinder temperature and cylinder wall temperature also increase the risk of quenching, further raising HC emissions.

Experiments were also performed using conventional CI combustion of fossil Diesel at similar load points. The specific HC emissions in this case were 0.06 g/kWh, and were thus much lower than those achieved using partially premixed combustion.

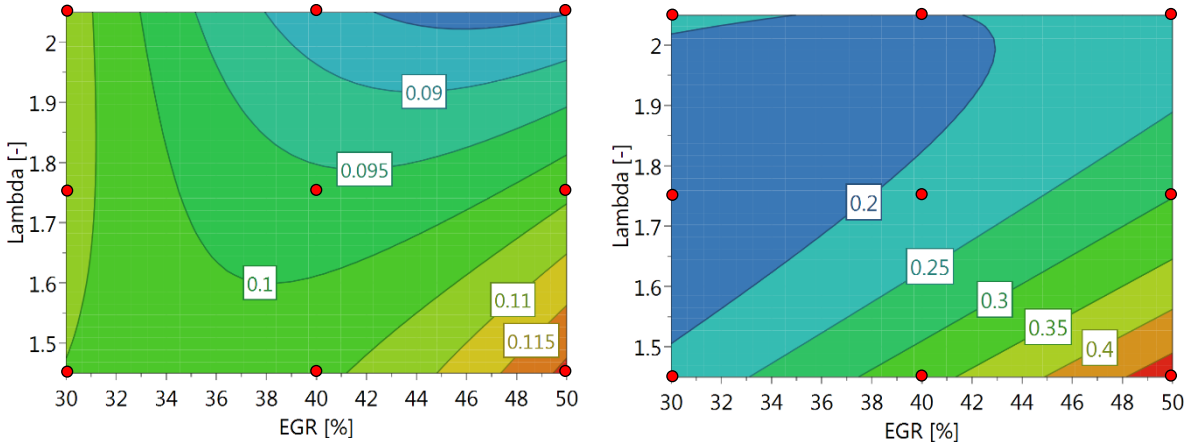

a) nBu30 b) nBu60

Figure 4-26 Partially premixed combustion indicated HC emissions of a) nBu30 and b) nBu60 at an engine speed of 1280 rpm and IMEP of 0.96 MPa in the LD engine.

4.3 Cold start

There are concerns about the poor cold start capability of alcohol blended fuels due to the reduction in the ignition attribute [37]. To assess renewable fuels comprehensively, cold start experiments were conducted in Volvo Cars' laboratory.

Figure 4-27 compares engine speed profiles observed using Diesel, nBu20H and 2EH30H during cold starts with the same target speed and control strategy at -25°C. All three fuels yielded similar engine speed curves, with the engine speed increasing to 1500 rpm within a second of the start signal and then falling rapidly and stabilizing. All tested fuels achieved a stable target speed around 1.5 seconds after the start signal.

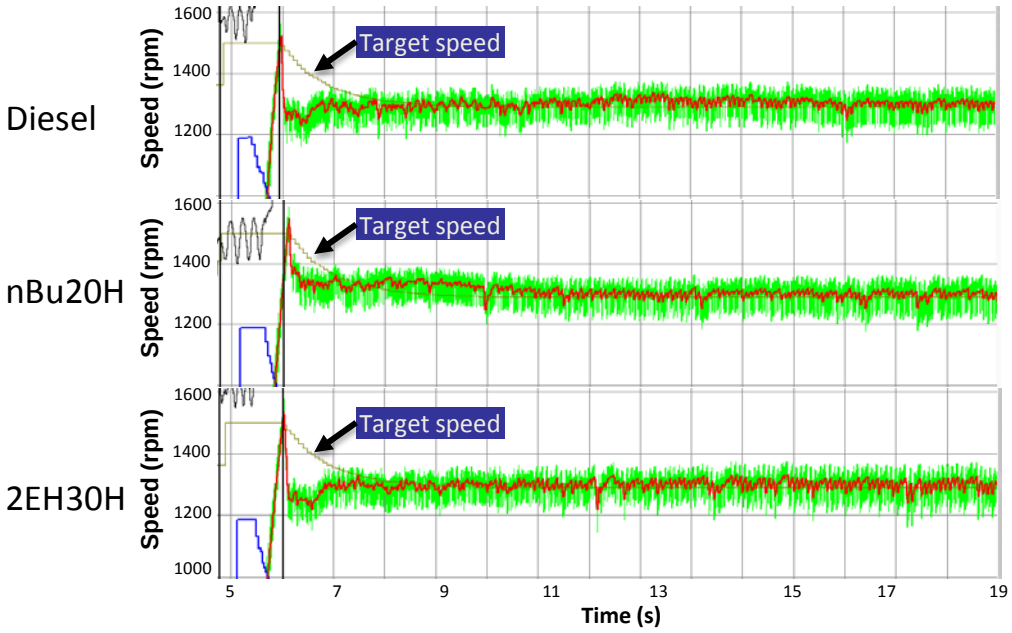

Figure 4-27 Engine speed during cold start experiments. Taken from Volvo Cars' report.

The nBu30H and 2EH30H blends (nBu20H in particular) exhibited better cold start behaviour than Diesel in that they caused the engine's speed to fall more smoothly after peaking because of their more favourable cold start properties.

Table 4-1 shows the properties of the fuels tested in the cold start experiments. The blends had lower cloud points and cold filter plugging point than Diesel fuel, both of which are beneficial during cold starts. The nBu20H blend also had slightly better idling stability than the other fuels because of its higher volatility and lower viscosity.

Table 4-1 Cold start properties of fuels

Properties	Unit	Diesel	Bu20H	2EH30H
Viscosity @ 40 °C	mm^2/s	3.037	2.444	3.033
Cloud point	°C	-9	-16	-18
Cold filter plugging point	°C	-25	-35	-36
Flash point	°C	82	38	73
C:H:O ratio	-	12:23:-	25:53:1	26:54:1

Experiments were also performed at 0, -10, -20 and -30 °C. The engine satisfied Volvo Car's start time requirements for all three fuels and at all test temperatures.

5 Conclusions

This thesis investigated the possibility of using alcohols and HVO as alternative fuels for Diesel engines in conventional CI combustion and partially premixed combustion systems. Four oxygenated alcohols (*n*-butanol, isobutanol, *n*-octanol, and 2-ethylhexanol) were blended with fossil Diesel, HVO, and RME, to create blends with known cetane numbers. Experiments were performed using both HD and LD single-cylinder Diesel engines, using fuels with CNs of 52 for conventional CI combustion and 36 or 26 for partially premixed combustion. Some tested fuels were selected also for fundamental spray experiments in a constant volume combustion chamber.

5.1 Engine tests

In conventional CI combustion, alcohol/Diesel blends and fossil-free blends with the same CN as Diesel exhibited Diesel-like ignition delays, SOC timings, and heat release profiles under all operating conditions in both HD and LD engines. The presence of alcohol in the fuel promoted combustion and reduced the combustion duration slightly.

Alcohol blends yielded indicated thermal efficiencies similar to or slightly greater than those for fossil Diesel, especially at intermediate and high load. The observed increases were attributed to the shortened combustion duration.

Soot emissions clearly decreased as the fuel's oxygen content increased; reductions of up to 84% and 51 % were seen in the HD and LD engines, respectively. Fuel-borne oxygen plays a central role in reducing soot emissions during conventional CI combustion because it reduces the equivalence ratio and promotes oxidation of soot precursors. Partial replacement of fossil Diesel fuel with aromatic-free HVO therefore reduces soot emissions.

In both LD and HD engines, the total PM number larger than 23 nm was reduced when using alcohol blends. In general, the diameter of emitted PM decreased as the fuel's oxygen content increased.

Replacing fossil Diesel with alcohol blends made combustion slightly faster and so increased NO_x emissions. In addition, DTBP-containing bends produced slightly higher NO emissions than HVO-containing blends. Because the alcohol blends had higher oxygen contents than fossil Diesel, their combustion yielded lower CO emissions, mirroring the trends seen for soot emissions. However, no significant effect of using alcohol blends on HC emissions relative to those achieved with fossil Diesel.

Compared to the standard piston, the wave piston reduced the combustion duration for both fossil Diesel and the oxygenated blends. This increased the thermal efficiency for fossil Diesel. The wave piston reduced PN, soot and CO emissions but increased NO_x emissions by improving the recirculating flow of fuel jets and enhancing soot oxidation. However, at the tested operating points, the wave design's beneficial effects on thermal efficiency for oxygenated fuels were appreciably weaker than those seen with fossil Diesel fuel.

At temperatures of 0 and -10 °C, all fuels showed comparable start and idling stabilities. At temperatures of -20, -25 and -30 °C, the nBu20H blend achieved slightly better idling stability than the other fuels.

Overall, the results show that from a combustion point of view, it is possible to use renewable fuels such as *n*-butanol, isobutanol, *n*-octanol, and 2-ethylhexanol, mixed with Diesel and ignition improvers or even fossil-free blends in existing Diesel engines without needing engine modifications.

Low CN fuels achieved partially premixed combustion much more readily than higher CN fuels at intermediate or high EGR rates. It seems that in LD Diesel engines, intermediate CN fuels (CN = 36) are more suitable for combustion at low loads with relatively high boost pressures, while low CN fuels (CN = 26) are more suitable for higher load combustion.

When using PPC, low CN fuels generated lower soot and NO emissions than they did under conventional CI combustion, but also produced higher CO and HC emissions. PPC also generated high variation in IMEP and pressure rise rates, both of which are significant challenges to its wider use. However, the drawbacks of violent combustion could be partially mitigated by using a multi-injection strategy. The potential benefits of PPC were demonstrated by the fact that it increased gross indicated thermal efficiency by up to 52 % (and by over 50 % in all tested conditions). Even when the pressure rise rate was capped at 6 bar/CAD, PPC offered very substantial increases in thermal efficiency compared to conventional CI combustion.

Table 5-1 summarises the average emissions and thermal efficiencies achieved with the tested fuels in the LD and HD engines under reference operating condition. The averaged values shown in the table are based on percentage changes relative to results obtained with fossil Diesel. A single arrow denotes a difference of 0 – 10 % differences or a statistically non-significant difference; two arrows denote a difference of 10 – 50 %; and three arrows denote a difference of more than 50 % compared to conventional CI combustion of fossil Diesel. The results shown in the "low CN blends" column are based on experiments using the nBu60D40 blend and partially premixed combustion in the LD engine under the reference operating conditions.

Table 5-1 Summary of average emissions and thermal efficiencies for various tested fuels in HD and LD engines

	Blends with HVO	Blends with DTBP	Low CN blends	Fossil-free
Soot emissions	↓↓↓	↓↓↓	↓↓↓	↓↓↓
NO_x emissions	↑	↑↑	↓↓↓	↑↑
CO emissions	↓↓	↓↓	↑↑↑	↓↓
HC emissions	↑	↑	↑↑↑	↓
Total PM concentration	↓↓	↓↓	-	↓↓↓
Thermal efficiency	↑	↑	↑	↑

5.2 Constant volume combustion chamber tests

The tested fuels all exhibited similar vapour phase penetration, but their liquid penetration was more sensitive to physical fuel properties such as the fuel's boiling point. HVO yielded slightly longer liquid penetration than Diesel.

The strong correlation between the flame lift-off length and the ignition delay was confirmed by testing fuel blends with different cetane numbers and oxygen contents. Generally, fuels with longer ignition delays had longer flame lift-off lengths. However, high CN values weren't always indicative of short ignition delays because the ignition delay also depends on the operating conditions and the method used to determine the CN.

As expected, the flame lift-off length was closely related to the soot optical thickness and soot volume fraction distribution, with longer flame lift-off lengths being associated with lower soot emissions. In addition to the flame lift-off length, soot formation depended strongly on the ignition delay, the oxygen mass fraction in the fuel, and the stoichiometric ratio.

6 Future work

The thesis describes an investigation into the scope for using alcohol/Diesel blends and fossil-free blends in conventional compression ignition combustion or partially premixed combustion. The study approved the application possibility from the combustion point of view. The evaluation of fuel deposit and engine durability tests could be concerned when using new fuels in the next step.

The future emissions legislation on particulate number may include even smaller particle size, therefore, the investigation on the great variation of small particle concentration for oxygenated fuels would be attractive and important.

References

[1] International Energy Agency, “Global EV Outlook 2018”, 2018.

[2] Wards Intelligence, http://subscribers.wardsintelligence.com/analysis/world-vehicle-population-rose-46-2016, 2017.

[3] European Automobile Manufacturers' Association, “ACEA Report: Vehicles in Use – Europe,” 2018.

[4] Eurostat, “Greenhouse Gas Emission Statistics - Emission Inventories,” 2018.

[5] United States Environmental Protection Agency, “Inventory of U.S. Greenhouse Gas Emissions and Sinks: 1990–2016,” 2018.

[6] European Commission, “Analysis of Options beyond 20% GHG Emission Reductions: Member State results,” 2012.

[7] European Commission, “European Council 23/24 October 2014 – Conclusions,” 2014.

[8] European Commission, “A Roadmap for Moving to a Competitive Low Carbon Economy in 2050,” 2011.

[9] BP Distribution Services, “BP Statistical Review of World Energy June 2015,” http://bp.com/statisticalreview, accessed Nov. 2015.

[10] European Commission, “EU Energy in Figures – Statistical Pocketbook 2018,” 2018.

[11] European Commission, “Renewable Energy – Recast to 2030 (RED II),” 2018.

[12] Swedish Riksdag, “The Climate Policy Framework,” 2017.

[13] China’s Ntional Energy Administration, “关于扩大生物燃料乙醇生产和推广使用车用乙醇汽油的实施方案”, 2017.

[14] A. Pires and R. Schechtman, “International Biofuels Policies,” Ethanol and Bioelectricity: Sugarcane in the Future of the Energy Matrix, 2010.

[15] R. Gray and B. Evans, “Biofuels Annual Canada Biofuels Annual 2013,” 2013.

[16] European Commission, “Energy Roadmap 2050,” 2012.

[17] S. Brynolf, M. Taljegard, M. Grahn, J. Hansson, “Electrofuels for the Transport Sector: A Review of Production Costs,” Renew. Sustain. Energy Rev., 81(2017):1887-1905, 2018.

[18] M. Ni, D. Y. C. Leung, and M. K. H. Leung, “A Review on Reforming Bio-Ethanol for Hydrogen Production,” Int. J. Hydrogen Energy, 32(15):3238–3247, 2007.

[19] C. Jin, M. Yao, H. Liu, C. Lee et al., “Progress in the Production and Application of N-butanol as a Biofuel,” Renewable and Sustainable Energy Reviews, 15:4080–4106, 2011.

[20] Directive 2009/28/EC of the European Parliament and of the Council, 2009.

[21] A. Morone and R.A. Pandey, “Lignocellulosic Biobutanol Production: Gridlocks and Potential Remedies,” Renewable and Sustainable Energy Reviews, 37:21–35, 2014.

[22] K. Munch, T. Zhang, “A Comparison of Drop-In Diesel Fuel Blends Containing Heavy Alcohols Considering Both Engine Properties and Global Warming Potentials,” SAE Technical Paper, 2016-01-2254, 2016.

[23] S. Kumar, J. H. Cho, J. Park, I. Moon, “Advances in Diesel–alcohol Blends and Their Effects on the Performance and Emissions of Diesel Engines,” Renewable and Sustainable Energy Reviews, 22:46–72, 2013.

[24] X. Gu, G. Li, X. Jiang, Z. Huang et al., “Experimental Study on the Performance of and Emissions from a Low-speed Light-duty Diesel Engine Fueled with n-Butanol–Diesel and Isobutanol–Diesel Blends,” Proc IMechE Part D: J Automobile Engineering, 227(2):261–271, 2013.

[25] M. Lapuerta, R. Garcia-Contreras, J. Campos-Fernandez, and M. Pilar Dorado, “Stability, Lubricity, Viscosity, and Cold-Flow Properties of Alcohol-Diesel Blends,” Energy & Fuels, 24:4497–4502, 2010.

[26] B. Heuser, T. Laible, M. Jakob, F. Kremer et al., “C8-Oxygenates for Clean Diesel Combustion,” SAE Technical Paper, 2014-01-1253, 2014.

[27] J. Campos-Fernandez, J. M. Arnal, J. Gomez, N. Lacalle et al., “Performance Tests of a Diesel Engine Fueled with Pentanol/Diesel Fuel Blends,” Fuel, 107:866–872, 2013.

[28] J. Trost, L. Zigan, A. Leipertz, “Quantitative Vapor Temperature Imaging in DISI-Sprays at Elevated Pressures and Temperatures using Two-Line Excitation Laser-Induced Fluorescence,” Proc. Combust. Inst., 34(2):3645–3652, 2013.

[29] A. Demirbas, “Biofuels Sources, Biofuel Policy, Biofuel Economy and Global Biofuel Projections,” Energy Convers. Manag., 49,(8):2106–2116, 2008.

[30] K. Lehto, A. Vepsäläinen, U. Kiiski, M. Kuronen, “Diesel Fuel Lubricity Comparisons with HFRR and Scuffing Load Ball-on-Cylinder Lubricity Evaluator Methods,” SAE Int. J. Fuels Lubr., 7(3):2014-01-2761, 2014.

[31] H. Aatola, M. Larmi, T. Sarjovaara, “Hydrotreated Vegetable Oil (HVO) as a Renewable Diesel Fuel: Trade-off between NOx, Particulate Emission, and Fuel Consumption of a Heavy Duty Engine.” SAE Technical Paper, 2008-01-2500, 2008.

[32] K. Sugiyama, I. Goto, K. Kitano, K. Mogi, “Effects of Hydrotreated Vegetable Oil (HVO) as Renewable Diesel Fuel on Combustion and Exhaust Emissions in Diesel Engine,” SAE Int. J. Fuels Lubr. 5:205–217, 2012.

[33] N. Noguchi, H. Terao, C. Sakata, “Performance Improvement by Control of Flow Rates and Diesel Injection Timing on Dual-Fuel Engine with Ethanol,” Bioresour. Technol., 56(1):35–39, 1996.

[34] H. Liu, X. Wang, Z. Zheng, J. Gu, H. Wang et al., “Experimental and Simulation Investigation of the Combustion Characteristics and Emissions using n-Butanol / Biodiesel Dual-Fuel Injection on a Diesel Engine,” Energy, 74:741–752, 2014.

[35] X. Lü, Y. Hou, L. Zu, and Z. Huang, “Experimental Study on the Auto-ignition and Combustion Characteristics in the Homogeneous Charge Compression Ignition (HCCI) Combustion Operation with Ethanol/n-heptane Blend Fuels by Port Injection,” Fuel, 85(2006):2622–2631, 2006.

[36] Z. Chen, J. Liu, Z. Wu, C. Lee, “Effects of Port Fuel Injection (PFI) of n-Butanol and EGR on Combustion and Emissions of a Direct Injection Diesel Engine,” Energy Convers. Manag., 76:725–731, 2013.

[37] R. Michikawauchi, S. Tanno, Y. Ito, M. Kanda, “Combustion Improvement of Diesel Engine by Alcohol Addition - Investigation of Port Injection Method and Blended Fuel Method,” SAE Technical Paper, 2011-01-0336, 2013.

[38] J. Campos-Fernández, J. Arnal, J. Gómez, M. Pilar Dorado, “A Comparison of Performance of Higher Alcohols/diesel Fuel Blends in a Diesel Engine,” Applied Energy, 95: 267–275, 2012.

[39] Ö. Can, I. Çelikten, N. Usta, “Effects of Ethanol Addition on Performance and Emissions of a Turbocharged Indirect Injection Diesel Engine Running at Different Injection Pressures,” Energy Convers. Manag., 45(2004):2429–2440, 2004.

[40] D. C. Rakopoulos, C. D. Rakopoulos, R.G. Papagiannakis, D.C. Kyritsis, “Combustion Heat Release Analysis of Ethanol or n-Butanol Diesel Fuel Blends in Heavy-Duty DI Diesel Engine,” Fuel, 90:1855–1867, 2011.

[41] D. C. Rakopoulos, C. D. Rakopoulos, E. G. Giakoumis, A. M. Dimaratos et al., “Effects of Butanol–Diesel Fuel Blends on the Performance and Emissions of a High-speed DI Diesel Engine,” Energy Conversion and Management, 51:1989–1997, 2010.

[42] Z. Xiao, N. Ladommatos, H. Zhao, “The Effect of Aromatic Hydrocarbons and Oxygenates on Diesel Engine Emissions,” Proc. Inst. Mech. Eng. Part D-Journal Automob. Eng., 214:307–332, 2000.

[43] E. Sukjit, J. M. Herreros, K. D. Dearn, R. García-Contreras et al., “The Effect of the Addition of Individual Methyl Esters on the Combustion and Emissions of Ethanol and Butanol-Diesel Blends,” Energy, 42,(1):364–374, 2012.

[44] G. Valentino, S. Merola, L. Marchitto, C. Tornatore, “Butanol-Diesel Blend Spray Combustion Investigation by UV-Visible Flame Emission in a Prototype Single Cylinder Compression Ignition Engine,” SAE Int. J. Engines, 8(5):2015–24–2435, 2015.

[45] H. Wu, K. Nithyanandan, J. Zhang, Y. Lin et al., “Impacts of Acetone – Butanol – Ethanol (ABE) Ratio on Spray and Combustion Characteristics of ABE – Diesel Blends,” Appl. Energy, 149:367–378, 2015.

[46] C. D. Rakopoulos, D. C. Rakopoulos, E. G. Giakoumis, D. C. Kyritsis, “The Combustion of n-Butanol/Diesel Fuel Blends and its Cyclic Variability in a Direct Injection Diesel Engine,” Proc. Inst. Mech. Eng. Part A J. Power Energy, 225(3):289–308, 2011.

[47] G. Valentino, F. E. Corcione, S. E. Iannuzzi, S. Serra, “Experimental Study on Performance and Emissions of a High Speed Diesel Engine Fuelled with n-Butanol Diesel Blends under Premixed Low Temperature Combustion,” Fuel, 92(1):295–307, 2012.

[48] G. Valentino, F. E. Corcione, S. Iannuzzi, U. Cagliari, “An Experimental Analysis on Diesel / n-Butanol Blends Operating in Partial Premixed Combustion in a Light Duty Diesel Engine,” SAE Technical Paper, 2012-01-1127, 2012.

[49] M. Yao, H. Wang, Z. Zheng, Y. Yue, “Experimental Study of n-Butanol Additive and Multi-Injection on HD Diesel Engine Performance and Emissions.” Fuel, 89:2191–2201, 2010.

[50] Q. Zhang, M. Yao, Z. Zheng, H. Liu et al. “Experimental Study of n-Butanol Addition on Performance and Emissions with Diesel Low Temperature Combustion.” Energy, 47:515–521, 2012.

[51] O. Armas, R. García-Contreras, Á. Ramos, “Pollutant Emissions from Engine Starting with Ethanol and Butanol Diesel Blends,” Fuel Process. Technol., 100:63–73, 2012.

[52] O. Armas, R. García-Contreras, Á. Ramos, “Pollutant Emissions from New European Driving Cycle with Ethanol and Butanol Diesel Blends,” Fuel Process. Technol., 122:64–71, 2014.

[53] T. Johnson, “Diesel Emission Control in Review,” SAE Int. J. Fuels Lubr. 1(1):68-81, 2009.

[54] C. Noehre, M. Andersson, B. Johansson, A. Hultqvist, “Characterization of Partially Premixed Combustion,” SAE Technical Paper, 2006-01-3412, 2006.

[55] V. Soloiu, M. Duggan, S. Harp, B. Vlcek, D. Williams, “PFI (port fuel injection) of n-Butanol and Direct Injection of Biodiesel to Attain LTC (Low-Temperature Combustion) for Low-Emissions Idling in a Compression Engine,” Energy, 52:143–154. 2013.

[56] H. Solaka, M. Tuner, B. Johansson, “Analysis of Surrogate Fuels Effect on Ignition Delay and Low Temperature Reaction during Partially Premixed Combustion,” SAE Technical Paper, 2013-01-0903, 2013.

[57] C. J. Leermakers, P. C. Bakker, L. M. T. Somers, L. P. H. Goey et al., “Butanol-Diesel Blends for Partially Premixed Combustion,” SAE Int. J. Fuels Lubr., 6(1): 217–229, 2013.

[58] F.Yang, C. Yao, J. Wang, M. Ouyang, “Load expansion of a dieseline compression ignition engine with multi-mode combustion,” Fuel, 171: 5–17, 2016.

[59] A. M. Ickes, S. V Bohac, D. N. Assanis, “Effect of Fuel Cetane number on a Premixed Diesel Combustion Mode,” Int. J. Engine Res., 10(4):251–263, 2009.

[60] N. Ladommatos, M. Parsi, A. Knowles, “The Effect of Fuel Cetane Improver on Diesel Pollutant Emissions,” Fuel, 75(1):8–14, 1996.

[61] L. J. Cunningham, T. J. Henly, A. M. Kulinowski, “The Effects of Diesel Ignition Improvers in Low-Sulfur Fuels on Heavy-Duty Diesel Emissions,” SAE Technical Paper, 902173, 1990.

[62] X. Li, W. L. Chippior, Ö. L. Gülder, “Effects of Fuel Properties on Exhaust Emissions from the Latest Light-Duty DI Diesel Engine,” SAE Technical Paper, 962116, 1996.

[63] Y. Kidoguchi, C. Yang, R. Kato, K. Miwa, “Effects of Fuel Cetane Number and Aromatics on Combustion Process and Emissions of a Direct-Injection Diesel Engine,” JSAE Rev., 21:469–475, 2000.

[64] L. Xing-Cai, Y. Jian-Guang, Z. Wu-Gao, H. Zhen, “Effect of Cetane Number Improver on Heat Release Rate and Emissions of High Speed Diesel Engine Fueled with Ethanol-Diesel Blend Fuel,” Fuel, 83(14–15):2013–2020, 2004.

[65] X. C. Lü, J. G. Yang, W. G. Zhang, Z. Huang, “Improving the Combustion and Emissions of Direct Injection Compression Ignition Engines using Oxygenated Fuel Additives Combined with a Cetane Number Improver,” Energy and Fuels, 19(5):1879–1888, 2005.

[66] Y. İçıngür, D. Altiparmak, “Effect of Fuel Cetane Number and Injection Pressure on a DI Diesel Engine Performance and Emissions,” Energy Convers. Manag., 44(3):389–397, 2003.

[67] G. Knothe, A. C. Matheaus, T. W. Ryan, “Cetane Numbers of Branched and Straight-Chain Fatty Esters Determined in an Ignition Quality Tester,” Fuel, 82(8):971–975, 2003.

[68] G. Knothe, “Dependence of Biodiesel Fuel Properties on the Structure of Fatty Acid Alkyl Esters,” Fuel Process. Technol., 86(10):1059–1070, 2005.

[69] A. Sudholt, L. Cai, J. Heyne, F. M. Haas et al., “Ignition Characteristics of a Bio-Derived Class of Saturated and Unsaturated Furans for Engine Applications,” Proc. Combust. Inst., 35(3):2957–2965, 2015.

[70] O. Ramadan, G. Webster, L. Menard, A. Wilcox et al., “Ignition Quality Tester (IQT ™) Precision Improvements from Using the Totally Automated Laboratory Model (TALM) Technology : Technology Update , Part-2 : Mini Inter- Laboratory Study Using the IQT ™ -TALM,” SAE Technical Paper, 2015-01-0805, 2015.

[71] L. N. Allard, G. D. Webster, T. W. Ryan, G. Baker et al., “Analysis of the Ignition Behaviour of the ASTM D-613 Primary Reference Fuels and Full Boiling Range Diesel Fuels in the Ignition Quality Tester (IQT) - Part III,” SAE Paper, 1999–01–3591, 1999.

[72] S. Bezergianni, A. Dimitriadis, “Comparison between Different Types of Renewable Diesel,” Renew. Sustain. Energy Rev., 21:110–116, 2013.

[73] P. Ghosh, S. B. Jaffe, “Detailed Composition-Based Model for Predicting the Cetane Number of Diesel Fuels,” Ind. Eng. Chem. Res., 45:346–351, 2006.

[74] Eric Sattler, “Comparing Methods to Determine Cetane Ratings of Fuel Blends,” U.S. Army Tank Automotive Research, Development and Engineering Center, U.S. Army Research, Development and Engineering Command. 2009.

[75] K. Lehto, A. Vepsäläinen, U. Kiiski, M. Kuronen, “Diesel Fuel Lubricity Comparisons with HFRR and Scuffing Load Ball-on-Cylinder Lubricity Evaluator Methods,” SAE Int. J. Fuels Lubr., 7(3):2014-01-2761, 2014.

[76] S. Berkhous, “Using A Constant Volume Combustion Chamber Analyzer For Predicting Derived Cetane Number Of Aviation Turbine Fuels,” IASH Paper, 2009.

[77] S. Kumar, J. H. Cho, J. Park, I. Moon, “Advances in Diesel-Alcohol Blends and their Effects on the Performance and Emissions of Diesel Engines,” Renew. Sustain. Energy Rev., 22:46–72, 2013.

[78] S. S. S. Popuri, R. M. Bata, “A Performance Study of Iso-Butanol-, Methanol-, and Ethanol-Gasoline Blends Using a Single Cylinder Engine,” SAE Tech. Pap. 932953, 1993.

[79] C. Leermakers, P.C. Bakker, L.M.T. Somers, L.P.H. Goey et al., "Butanol-Diesel Blends for Partially Premixed Combustion," SAE Int. J. Fuels Lubr. 6(1): 2013-01-1683, 2013.

[80] J. Eismark, “The Role of Piston Bowl Shape in Controlling Soot Emissions from Heavy-Duty Diesel Engines,” Gothenburg; 2018.

[81] C. Du, M. Andersson, and S. Andersson, “The Influence of Ethanol Blending in Diesel Fuel on the Spray and Spray Combustion Characteristics,” SAE Int. J. Fuels Lubr., 7(3):823–832, 2014.

[82] C. Du, S. Andersson, M. Andersson, “Two-dimensional Measurements of Soot in a Turbulent Diffusion Diesel Flame : the Effects of Injection Pressure, Nozzle Orifice Diameter, and Gas Density,” Combust. Sci. Technol, 2018.

[83] T. Zhang, K. Munch, and I. Denbratt, “An Experimental Study on the Use of Butanol or Octanol Blends in a Heavy Duty Diesel Engine,” SAE Int. J. Fuels Lubr., 8(3):2015-24–2491, 2015.

[84] G. Woschni, “A Universally Acceptable Equation for the Instantaneous Heat Transfer Coefficient in the Internal Combustion Engine,” SAE Technical Paper. 670931, 1967.

[85] Economic Commission for Europe, “Proposal for Draft Amendment 3 to Global Technical Regulation (GTR) No. 4: Test Procedure for Compression-Ignition (C.I.) Engines and Positive-Ignition (P.I.) Engines Fuelled with Natural Gas (NG) or Liquefied Petroleum Gas (LPG) with Regard to the Emission of Pollutants,” 2014.

[86] Commission Directive 2005/78/EC, 2005.

[87] R. S. Spindt, “Air-Fuel Ratios from Exhaust Gas Analysis,” SAE Pap., 788–793, 1965.

[88] J. Yon, R. Lemaire, E. Therssen, P. Desgroux, A. Coppalle, K. Ren, “Examination of Wavelength Dependent Soot Optical Properties of Diesel and Diesel/rapeseed Methyl Ester Mixture by Extinction Spectra Analysis and LII Measurements,” Appl. Phys. B, 104, 253–271, 2011.

[89] M. Choi, G. Mulholland, A. Hamins, T. Kashiwagi, “Comparisons of the Soot Volume Fraction Using Gravimetric and Light Extinction Techniques,” Combust. Flame, 102:161–169, 1995.

[90] J. B. Heywood, “Internal combustion engine fundamentals,” New York: McGraw-Hill; 1988.

[91] J. E. Dec, “A Conceptual Model of DI Diesel Combustion Based on Laser-Sheet Imaging,” SAE Technical Pape, 970873, 1997.

[92] C. J. Mueller, W. J. Pitz, L. M. Pickett, G. C. Martin, D. L. Siebers, C. K. Westbrook, “Effects of Oxygenates on Soot Processes in DI Diesel Engines: Experiments and Numerical Simulations,” SAE Technical Pape, 2003-01-1791, 2003.

[93] S.E. Iannuzzi, G. Valentino, “Comparative Behavior of Gasoline-Diesel/Butanol-Diesel Blends and Injection Strategy Management on Performance and Emissions of a Light Duty Diesel Engine,” Energy, 71:321–331, 2014.

[94] G. Chen, Y. Shen, Q. Zhang, M. Yao et al., “Experimental Study on Combustion and Emission Characteristics of a Diesel Engine Fueled with 2,5-Dimethylfuran-Diesel, n-Butanol-Diesel and Gasoline-Diesel Blends,” Energy, 54:333–342, 2013.

[95] L. M. Pickett, D. L. Siebers, “Soot in Diesel Fuel Jets : Effects of Ambient Temperature, Ambient Density, and Injection Pressure,” Combust. Flame, 138(2004):114–135, 2004.

[96] N. Peters, “Turbulent Combustion,” Cambridge University Press, Cambridge, 2000

[97] H. Ghiassi, P. Toth, J. Lighty, “Sooting Behaviors of n-Butanol and n-Dodecane Blends,” Combustion and Flame, 161(3):671–679, 2012.

[98] L. M. Pickett, D. L. Siebers, and C. A. Idicheria, “Relationship between Ignition Processes and the Lift-Off Length of Diesel Fuel Jets,” SAE Technical Paper, 2005-01-3843, 2005.

[99] S. Kook, L. M. Pickett, “Soot Volume Fraction and Morphology of Conventional, Fischer-Tropsch, Coal-Derived, and Surrogate Fuel at Diesel Conditions,” SAE Int. J. Fuels Lubr., 5(2):2012-01–0678, 2012.

[100] M. Jakob, T. Hülser, A. Janssen, P. Adomeit, S. Pischinger, G. Grünefeld, “Simultaneous High-speed Visualization of Soot Luminosity and OH* Chemiluminescence of Alternative-fuel Combustion in a HSDI Diesel Engine under Realistic Operating Conditions,” Combust. Flame, 159(7):2516–2529, 2012.

[101] P. Hellier, N. Ladommatos, R. Allan, J. Rogerson, “The Influence of Fatty Acid Ester Alcohol Moiety Molecular Structure on Diesel Combustion and Emissions,” Energy and Fuels, 26(3):1912–1927, 2012.

[102] D.B. Kittelson, W.F. Watts, J.P. Johnson, “On-Road and Laboratory Evaluation of Combustion Aerosols-Part1: Summary of Diesel Engine Results,” J. Aerosol Sci., 37:913–930, 2006.

[103] G. Fontaras, M. Kousoulidou, G. Karavalakis, T. Tzamkiozis, P. Pistikopoulos et al., “Effects of Low Concentration Biodiesel Blend Application on Modern Passenger Cars. Part 1: Feedstock Impact on Regulated Pollutants, Fuel Consumption and Particle Emissions,” Environ. Pollut., 158(5):1451–1460, 2010.

[104] B. R. Kumar, S. Saravanan, D. Rana, V. Anish, A. Nagendran, “Effect of a Sustainable Biofuel – n-octanol – on the Combustion , Performance and Emissions of a DI Diesel Engine under Naturally Aspirated and Exhaust Gas Recirculation (EGR) Modes,” Energy Convers. Manag., 118:275–286, 2016.